



## Design Principals and Fundamental Understanding of Biosensors for Amyloid- $\beta$ Detection

Journal:	<i>Journal of Materials Chemistry B</i>
Manuscript ID	TB-REV-02-2020-000344.R1
Article Type:	Review Article
Date Submitted by the Author:	31-Mar-2020
Complete List of Authors:	Zhang, Yanxian; University of Akron, Chemical, Biomolecular, and Corrosion Engineering Ren, Baiping; University of Akron, Chemical, Biomolecular, and Corrosion Engineering Zhang, Dong; University of Akron, Chemical, Biomolecular, and Corrosion Engineering Liu, Yonglan; University of Akron, Chemical, Biomolecular, and Corrosion Engineering Zhang, Mingzhen; University of Akron, Chemical, Biomolecular, and Corrosion Engineering Zhao, Chao; The University of Alabama, Chemical and Biomolecular Engineering Zheng, Jie; University of Akron, Chemical, Biomolecular, and Corrosion Engineering

## **Design Principles and Fundamental Understanding of Biosensors for Amyloid- $\beta$ Detection**

Yanxian Zhang<sup>1</sup> $\zeta$ , Baiping Ren<sup>1</sup> $\zeta$ , Dong Zhang<sup>1</sup>, Yonglan Liu<sup>1</sup>, Mingzhen Zhang<sup>1</sup>,  
Chao Zhao<sup>2</sup>, and Jie Zheng<sup>1\*</sup>

<sup>1</sup>Department of Chemical, Biomolecular, and Corrosion Engineering  
The University of Akron, Ohio

<sup>2</sup> Department of Chemical and Biomolecular Engineering  
The University of Alabama, Alabama

$\zeta$  The authors contribute equally to this work.

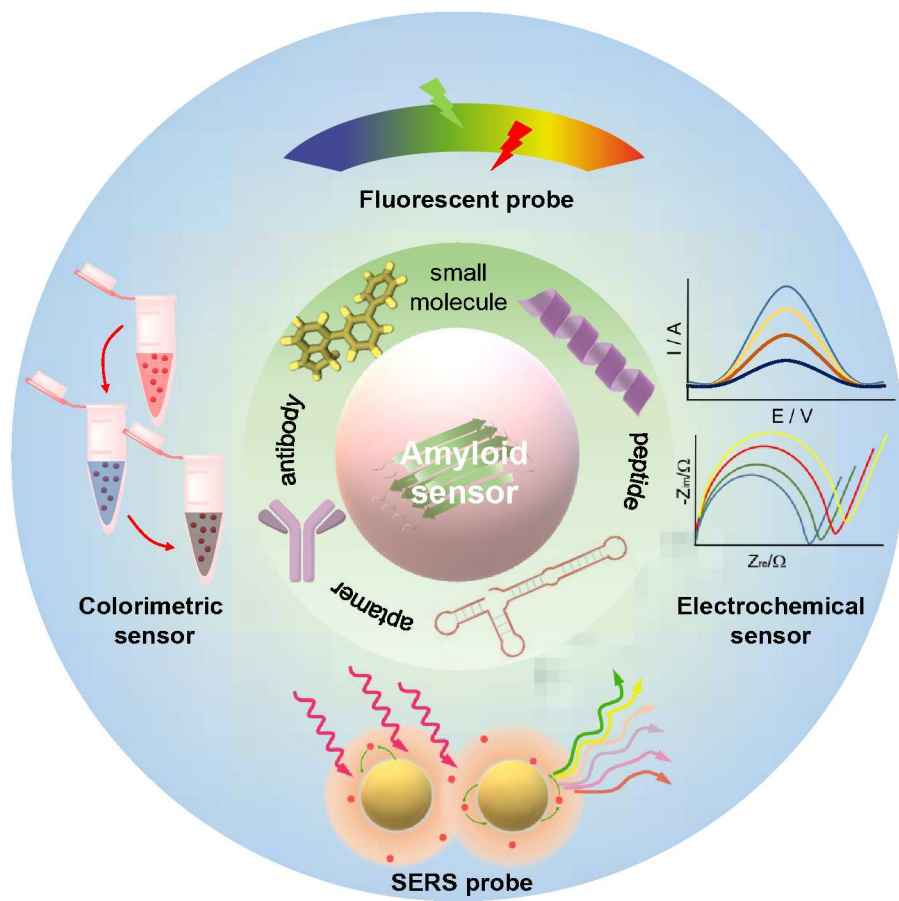
\* Corresponding author: [zhengj@uakron.edu](mailto:zhengj@uakron.edu)

### Abstract

Alzheimer disease (AD), as an age-related, progressive neurodegenerative disease, pose substantial challenges and burdens on public health and disease research. While significant research, investment, and progress have been made for the better understanding of pathological mechanisms and risk factors of AD, all clinical trials for AD treatment and diagnostics have failed so far. Since early and accurate diagnostics of AD is key to AD prevention and treatment, the development of probes for AD-related biomarkers is highly important but challenging for AD diagnosis. In this review, emerging evidence highlights the importance of A $\beta$  cascade hypothesis and indicates a significant role of A $\beta$  and their aggregates as biomarkers in the pathogenesis of AD, we present an up-to-date summary on A $\beta$ -based biosensor systems. Four typical biosensor systems for A $\beta$  detection and representative examples from each type of biosensors are carefully selected and discussed in terms of their sensing strategies, materials, and mechanisms. Finally, we address the remaining challenges and opportunities for the development of future sensing platforms for A $\beta$  detection and A $\beta$ -based diagnostics of AD.

**Keywords:** Alzheimer disease (AD), Amyloid- $\beta$  peptide, Biosensor, Neurodegenerative disease, Disease diagnostics, Bioprobe.

## Figure of Content



## 1. Introduction

Alzheimer's Disease (AD), as a most common aging-related neurodegenerative disorder, has affected millions of people worldwide and costed \$290 billion health care alone, but is currently incurable. Similar to other neurodegenerative diseases including Parkinson's disease (PD), Huntington's disease (HD), and type 2 diabetes (T2D), aging is considered as a main risk factor for AD due to natural selection and evolution. Longer life expectancy has led to an increased number of AD cases globally for the elders (>65 years old), which often suffer from the progressive loss of neuronal cells, leading to cognitive impairment, memory loss, and brain dysfunction. Apart from increasing age, other known risk factors for AD development include susceptibility genes, lifestyle choices (e.g. diet, exercise, and alcohol intake)<sup>1</sup>, environmental factors (e.g. pesticides and neurotoxic metals, such as lead, mercury, and arsenic)<sup>2, 3</sup>, and other diseases (e.g. head injuries, T2D, PD, and cardiovascular diseases)<sup>4, 5</sup>. The complex interplay between these risk factors makes the pathogenesis mechanisms of AD (e.g. A $\beta$  aggregation, tau hyperphosphorylation, cholinergic neuron damage, imbalanced inflammatory hypothesis, dysregulated energy metabolism, oxidative stress, and calcium dyshomeostasis) difficult to understand and study<sup>6</sup>. Numerous studies from neuropathology, genetics, and transgenic modeling have revealed the two compelling pathological hallmarks in the brains of AD patients: cerebral  $\beta$ -amyloidosis in the form of  $\beta$ -amyloid (A $\beta$ ) plaques<sup>7, 8</sup> and tauopathy in the form of neurofibrillary tangles<sup>9, 10</sup>. Different anti-AD strategies and drugs have been proposed and developed based on different AD hypotheses, however, FDA only approved two types of drugs - cholinesterase inhibitors (Aricept, Exelon, Razadyne) and memantine (Namenda) - to treat the cognitive symptoms (memory loss, confusion, and problems with thinking and reasoning) of AD, but not to cure AD or slow down the progress of AD.

The marginal benefits for current medical treatments of AD drive the parallel and significant efforts to develop diagnostic approaches for the early detection of AD and the monitoring of AD progress and disease status.<sup>11</sup> A generally accepted clinical criteria for AD diagnosis has three phases: an asymptomatic phase (AD without symptoms), a prodromal phase (AD with mild cognitive impairment), and a late-onset dementia (AD with irreversible neuron loss and brain damage). Early identifying preclinical and prodromal AD is critical for initiating symptomatic treatment before significant brain damage and neuronal loss become irreversible. Based on different pathogenic hypotheses of AD, different diagnostic strategies and techniques have been proposed and developed for the diagnosis and detection of AD-related biomarkers, including A $\beta_{40/42}$ , tau, phosphorylated tau, neurofilament light chain (NfL), vinisin-like protein 1 (VLP-1), neuron-specific enolase (NSE), heart fatty acid binding protein (HFABP), and glial activation (YKL-40)<sup>12-16</sup>. While it is still under hotly debated on the determination of pathologically-relevant AD-related biomarkers, controversial or inconsistent results for AD biomarkers make the early and accurate diagnostics of AD even more challenging. Among these AD-related biomarkers, there is also a strong consensus on "A $\beta$  cascade hypothesis" that the aggregation and deposition of misfolded A $\beta$  peptides into cytotoxic species are pathologically associated with AD (**Figure 1a**).

As shown in **Figure 1b**, rapid progress in using A $\beta$  biomarker for AD diagnostics has outpaced other AD biomarkers, as evidenced by almost 50% of a total of publications regarding A $\beta$  biomarker.

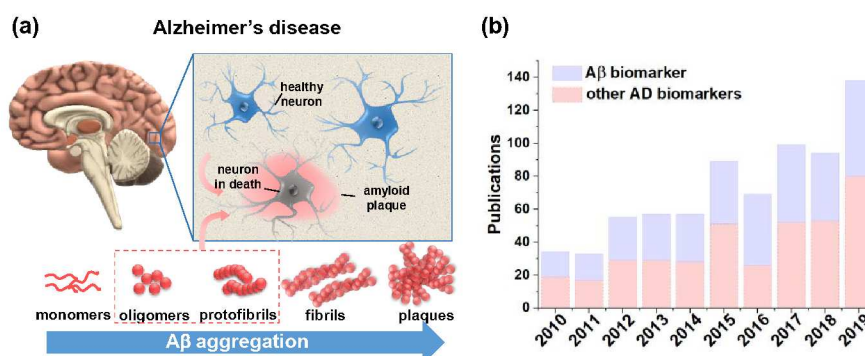


**Figure 1.** (a) Schematic illustration of “A $\beta$  cascade hypothesis” and pathological association between the deposition of A $\beta$  cytotoxic aggregates and Alzheimer’s disease. (b) Number of SCI-index papers in the field of the diagnosis of Alzheimer’s disease between 2010-2019, as searched by a combination of the keywords of “Alzheimer’s disease”, “detection”, “biomarker”, “ $\beta$ -amyloid”, and “NOT  $\beta$ -amyloid” in the topic of papers from the Web of Science database.

A general design strategy of biosensors for A $\beta$  detection is largely based on the sequential and structural features of A $\beta$  and its associated compounds, including (i) targeting primary, secondary, and final A $\beta$  aggregates along the progressive aggregation process<sup>17-19</sup>; (ii) targeting the metal ions that stabilize and accelerate A $\beta$  formation<sup>20-22</sup>; and (iii) targeting A $\beta$ -specific compounds that inhibit A $\beta$  production or promote A $\beta$  clearance<sup>23, 24</sup>. Among them, from a structural viewpoint, most of sensing probes (e.g. fluorescence chemicals, antibodies, aptamers, and peptides-based probes) are designed to detect A $\beta$  protofibrils, fibrils, and plaques (namely f-A $\beta$ ), all of which contain  $\beta$ -sheet-rich structure that could be used as specific structural motif for the probes to recognize and bind<sup>25, 26</sup>. Numerous computational and experimental studies<sup>27-29</sup> have reported several common binding sites of A $\beta$ , and eliminating those binding sites by mutations greatly diminished the photoluminescence, electric current, surface Raman scattering, and colorimetric response from the probe-A $\beta$  complexes. Generally, the A $\beta$ -targeting probes favor to bind to hydrophobic grooves (e.g. Met35-Val39, central hydrophobic cluster, and C-terminal region) of f-A $\beta$  along the long axis of the f-A $\beta$  via hydrophobic interactions<sup>30-32</sup>, to aromatic residues (e.g. Phe4, Tyr10, Phe19, Phe20) of f-A $\beta$  via  $\pi$ - $\pi$  stacking interactions<sup>33, 34</sup>, to some local planar surfaces via stacking interactions<sup>35, 36</sup>, to salt bridge between Asp23-Lys28 via electrostatic interactions<sup>37, 38</sup>. Upon binding to A $\beta$ , different A $\beta$ -targeting probes are able to induce the detectable signal changes in fluorescence, Raman scattering, impedance, or optical colors so as to lay down a foundation to fabricate different A $\beta$ -targeting biosensors. Additional techniques including surface enhanced Raman scattering (SERS), surface plasmon resonance (SPR) can further enhance signal expression upon binding of probes to A $\beta$ .

From a broader mechanistic view, the “A $\beta$  cascade hypothesis” can be generally applied to the “amyloid aggregation hypothesis”, which shows common pathological features to other protein-misfolding diseases, e.g. human islet polypeptide (hIAPP) aggregation is associated with T2D and  $\alpha$ -synuclein aggregation is associated with PD. This indicates that diagnostic strategies for AD could possibly apply to other neurodegenerative diseases, because these amyloid proteins share many structural, kinetic, and even cytotoxic characteristics during amyloid aggregation process.

In this review, on the basis of the A $\beta$  hypothesis and the significant roles of A $\beta$  in the pathogenesis of AD, we aim to summarize recent progress, challenges, and future direction in A $\beta$ -based (not other biomarkers-based) biosensors for A $\beta$  detection and AD diagnostics. This review mainly covers both fundamental principles and practical applications of A $\beta$ -based biosensors from design strategies, sensing materials, sensing mechanisms, to in vitro ad in vivo applications. This review does not intend (it is impossible) to provide comprehensive summary of all types of biosensors for A $\beta$  detection, but rather to focus on the most promising biosensors and the underlying sensing mechanisms, and some general principles for the design of sensing materials and methods for A $\beta$  detection. The sensing techniques cover photo-fluorescence, electrochemistry, surface-enhanced Raman scattering spectroscopy, and colorimetry for A $\beta$  detection and AD diagnostics, while sensing materials cover antibodies, aptamers, peptides, and small molecules, both of which are carefully presented, discussed, and summarized in **Table 1** and **Table 2**. Finally, we discuss some of the persistent technological/fundamental barriers that still remain, as well as offer some of opinions for future research directions that should be undertaken to overcome these barriers. Hopefully, this review will provide a different perspective to improve our understanding of A $\beta$  biomarker working mechanisms in relation to the pathogenesis of AD, which help to develop the early, accurate, and responsive detection of A $\beta$  for the effective diagnosis and treatment of AD at the early stage.

**Table 1.** A summary and classification of different types of amyloid- $\beta$  sensors

Type	Sensor	Target	Read-out	Binding affinity*/ Sensitivity	Ref.
Fluorescence probes	ThT	Insoluble amyloid aggregates	~480 nm	~ 580 nM*	39
	PiB		450-480 nm	~ 4.38 nM*	40
	IRI		~575 nm	~ 374 nM*	19
	NIAD-4		>600 nm	~ 10 nM*	41
	BODIPY7		~ 615 nm	~ 108 nM*	42
	DANIRs		~ 625 nm	~ 27 nM*	43
	BAP-1		~ 650 nm	~ 44 nM*	44
	CRANAD-2		715-805 nm	~ 38 nM*	45
	Styry-11		~ 770 nm	-	46
	BSPOTPE		~ 480 nm	-	23

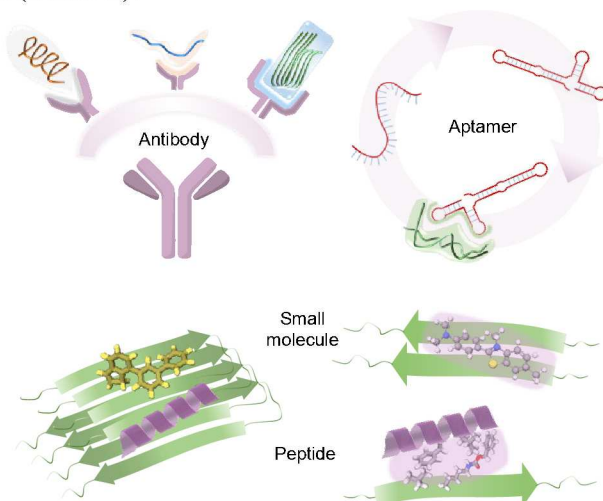
	TPE-TPP		450-480 nm	~ 580 nM*	47
	QM-FN-SO <sub>3</sub>		~ 720 nm	< 580 nM*	48
	BD-Oligo	Amyloid oligomer	~ 530 nm	~ 480 nM*	49
<b>Electro-chemical sensors</b>	Ab <sub>2</sub> -GOD@Ce:ZONFs-Lum/AgCys NWs	Aβ		11.5 pM	50
	GCE/MnCO <sub>3</sub> /PDDA/Au/HC-7/BSA/anti-Aβ	Aβ	ECL	4.4 fM	51
	GCE/Ru(bpy) <sub>3</sub> <sup>2+</sup> /zinc oxalate MOFs/Ab <sub>1</sub> /BSA	Aβ		3 fM	52
	MCH-aptamer-AuR	Aβ oligomer	EIS/CVs	30 pM	53
	Cu <sup>2+</sup> /aptamers/BSA/GE	Aβ <sub>16</sub> / Aβ <sub>40</sub>	ECL	35 fM	54
	AuNPs-PEDOT-PTAA/PrPC	Aβ oligomer	EIS	0.1 fM	55
	Poly(curcumin-Ni)	Aβ oligomer	EIS	1 pM	56
	OECT	Aβ aggregates	SWV	2.21 pM	57
	MCH/β-CD-Ag	Aβ oligomer	LSV	8 pM	58
		Au Nanoshells/Sialic Acid	Aβ		1 pM
<b>SERS sensors</b>	AgNGS <sub>[4-FBT]</sub>	Aβ	Raman spectra	55 fM	60
	PAapt-AuNPs	Aβ oligomer / tau		37 μM/0.42 fM	61
	RB-AuNPs	Aβ	Raman/FL 590nm	0.5 μM	62
<b>Colorimetric sensors</b>	AuNPs/Cu <sup>2+</sup>	Aβ <sub>40</sub>	Visible color change/absorption spectra	50 nM/ 0.6 nM	63
	CdTe/AuNPs/PrP(95-110)	Aβ oligomer		20 nM	64

## 2. Molecular Sensing Probes for Aβ Detection

Discovery and design of probes for Aβ detection require fundamental knowledge to understand the structural features of Aβ species at different aggregation stages so as to determine possible binding sites for probes to specifically recognize and bind to Aβ. Depending on the physical nature of Aβ (i.e. sizes, shapes, aggregation states) at different physiological conditions, it requires different probe materials and sensing strategies to achieve specific and sensitive binding to Aβ (**Figure 2**). Generally speaking, *in vivo* imaging probes (e.g. NIR imaging probes, fluorescence imaging probes, and single-photon emission computed tomography imaging probes) require sufficient BBB penetration ability for imaging Aβ plaques deposited in human brain, but it is still arguable that the correlation between Aβ plaques and neurodegenerative progress in AD brains is weak. Alternatively, *in vitro* or *ex vivo* probes (e.g. antibodies, aptamers, peptides) allow to detect probable early Aβ aggregates from cerebrospinal fluid (CSF) or blood, because Aβ aggregates in CSF or blood are more pathologically linked to AD severity. Many probes have been developed for Aβ-targeting detection, we classify them into four groups based on their molecular structures (i.e., nucleic acids, peptides, small molecules, and polymers) and typical probe examples for each group



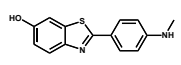
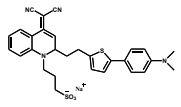
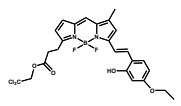
are summarized in (Table 2).



**Figure 2.** Different sensing probes for A $\beta$  detection.

**Table 2.** Molecular sensing probes for A $\beta$  detection<sup>48, 49,65-73</sup>

Category	Advantage	Disadvantage	Representative Probe Description		Binding affinity	Ref
Nucleic acids	High sensitivity and selectivity for low-quantity detection; able to be synthesized and modified with active groups; can be renatured	Rapid degradation (especially RNA aptamers). Can be degraded by nucleases in biological media like blood, easily digested by enzymes	DNA aptamer (- A $\beta_{40}$ oligomers)	5'-HS-GCCTGTGGT GTTGGGGCG GGTGCG-3'	25 nM	65
			RNA aptamer (- A $\beta_{fibrils}$ )	5'-HS-GCGTGTGGG GCTTGGGCA GCTGGG-3'		
			RNA aptamer (- A $\beta_{fibrils}$ )	5'-UUUACCGUA AGGCCUGUC UUCGUUUGA CAGCGGCUU GUUGACCCU CACACUUUG UACCUGCUG CCA-3'	29 nM	66
Peptides	High selectivity; high efficacy toward amyloid misfolding; high conformationa	Potential risk of denaturation, aggregation, and undesired adsorption; proteolytic instability; poor BBB	rPK-4 (- A $\beta_{42}$ oligomers)	KDKTPKSKSK	200 nM	67
			hIAPP <sub>8-18</sub> (- A $\beta_{40}$ )	ATQRLANFLV H	275 nM	68
			Rational designed	GTVWWG	840 nM	69

	flexibility	permeability	hexapeptide (-A $\beta_{42}$ )			
Small molecules	Highly stable; low cost, easy to be designed and modified with active groups	Low binding affinity; relatively low selectivity	PiB (- f-A $\beta$ )		20 nM	72
			QM-FN-SO <sub>3</sub> (- f-A $\beta$ )		< 580 nM	48
			BD-Oligo (-A $\beta$ oligomer)		480 nM	49
Polymers	High sensitivity and selectivity for low-quantity detection; able to recognize multiple or single epitope	High price and low stability; cannot be manually synthesized; likely to provoke undesirable immune responses; large molecular weight (~150 kDa)	Antibody (-A $\beta$ residue <sub>3-8</sub> )	6E10	nM ~ pM	70
			Antibody (-A $\beta_{40}$ fibril)	WO1		71
			Antibody (-A $\beta_{40/42}$ oligomer)	A11		73

## 2.1. Antibody-based probes

Antibody probes are mainly derived from immune system and functioned through the antibody-antigen interactions. Antibody is a large Y-shaped protein (also known as immunoglobulin), typically composed of one large heavy chain and two small symmetrical chain lying on the heavy chain. Natural selection makes the amino-terminal end of both light chains being served as common binding region (Fab, fragment antigen-binding region), which specifically targets its corresponding antigens to form stable antigen-antibody complex via spatial complementarity, dock-lock, and intermolecular non-covalent bonds<sup>74</sup>.

Highly specificity and sensitivity of the antigen-antibody interactions have long been used for the diagnosis and (immune)therapy of different diseases, including AD and other neurodegenerative diseases<sup>75, 76</sup>. Early studies on the immunization of transgenic mice with A $\beta$  peptide exhibited an inhibition effect on the progression of AD-like neuropathology, suggesting the possible humoral immune response to the pathogenesis of the disease<sup>77, 78</sup>. While more than 1:10,000 serum antibody titers against A $\beta_{42}$  were found<sup>77</sup>, later transgenic mice models and clinical trials only identified a much less number of anti-A $\beta$  antibodies capable for recognizing amyloid plaques in AD patient brains<sup>73</sup>. Among them, some anti-A $\beta$  antibodies<sup>79</sup> to recognize the sera in

the healthy adults were further identified, so that *in vitro* immortalization of cell lines derived from healthy subjects was established to produce these anti-A $\beta$  antibodies used for A $\beta$  probes<sup>80</sup>.

Most of A $\beta$ -antibodies (e.g. 6E10<sup>70</sup>, MOAB-2<sup>81</sup>) were designed to only target the specific residues of monomeric A $\beta$  or amorphous A $\beta$  aggregates, which are likely off-pathway AD species. Differently, conformational-specific A $\beta$ -antibodies were also developed to recognize the specific secondary structures (i.e. cross- $\beta$ -structure) of high-ordered A $\beta$  aggregates and fibrils<sup>71, 82, 83</sup>. The structural and conformational differences between unstructured A $\beta$  aggregates and highly-ordered A $\beta$  aggregates enable conformational-specific A $\beta$ -antibodies to recognize and distinguish them. These conformational-specific A $\beta$ -antibodies include WO1<sup>71</sup> for detecting A $\beta$  fibrils, A11<sup>73</sup> and F11G3<sup>84</sup> for detecting A $\beta$  oligomers. Antibodies for targeting A $\beta$  oligomers are particularly important for AD diagnostics and treatment, because A $\beta$  oligomers (e.g. spherical particles of 2.7-4.2 nm, linear strings, annular species) are well recognized as toxic and pathological species responsible for AD<sup>85</sup>.

## 2.2. Aptamer-based probes

Similar to antibodies, aptamers have superior binding sensitivity to targeted proteins. The short single-stranded DNA or RNA oligonucleotides can bind to proteins, small molecules, or cells at nano- to picomolar dissociation constant ( $K_d$ )<sup>86</sup>. However, different from antibody binding, aptamers are more structurally flexible to change their three-dimensional structures for better accommodating with targets. Aptamers can also be readily incorporated with functional compounds (e.g. fluorescent small molecules and biotins) to achieve additional imaging or to improve stability upon binding<sup>65</sup>.

Aptamers binding to A $\beta$  are generated *in vitro*, from a large pool of randomized nucleic acid sequences through the SELEX (systematic evolution of ligands by exponential enrichment) selection methodology. After exposing to A $\beta$ , A $\beta$ -targeting oligonucleotide sequences can be separated and synthesized to single stranded DNA/RNA aptamer<sup>87</sup>. However, the exact favorable binding sites between aptamers and A $\beta$  still remain largely unknown. Several studies have found that aptamers appear to have more favorable binding to A $\beta$  fibrils than A $\beta$  monomers or low-molecular-weight oligomers. This favorable binding behaviors of aptamers were also observed for other amyloid fibrils of  $\alpha$ -synuclein<sup>65, 88</sup>, prion proteins<sup>89, 90</sup>, tau protein<sup>91, 92</sup>, as well as ribonucleoprotein complexes (e.g. stress granules, RNA-processing organelles)<sup>93</sup>, indicating that a common  $\beta$ -sheet structure in these biomolecules (not limited to amyloid fibrils) is highly possible binding targets for aptamers<sup>94-96</sup>. Additional, loop regions of the stem-loop structured aptamer were also found to be involved and critical for recognizing and interacting with A $\beta$ <sup>97</sup>. Apart from the geometrically shape complementarity, due to negatively charged phosphate groups in aptamers, polyelectrolytic interactions between aptamer and A $\beta$  also provide binding driving forces and sites for A $\beta$  detection. Such polyelectrolytic interactions are not structurally specific, instead more chemically and generally applied to detect A $\beta$  aggregates of

different sizes, shapes, and interfacial properties.

While the exact binding mechanism of between aptamer and A $\beta$  is still not fully understood, several aptamers have been identified to target different aggregated states of A $\beta$ . A representative RNA-based aptamer can reactive with A $\beta$  fibrils, with the lowest  $K_d$  of 29 nM<sup>66</sup>. Another 39-nucleotide DNA aptamer (RNV95) was developed to probe tetrameric and pentameric A $\beta_{40}$  aggregates with 50-400 nM affinity<sup>18</sup>. Eight aptamers without sequence similarity (e.g. T-SO517: *GGTGG-CTGGA-GGGGG-CGCGA-ACG*, T-SO554: *CGAGG-GGCGT-CTGGG-AGTGG-TCGG*, T-SO504: *CAGGG-GTGGG-CAAAG-GGCCGG-TGGTG*, and T-SO508: *GCCTG-TGGTG-TTGGG-GCGGG-TGCG*), which were originally designed to target  $\alpha$ -synuclein with  $K_d$  of 68 nM, can also bind to A $\beta$  oligomers to form G-quadruplex structures, with the minimum  $K_d$  of 25 nM, comparable to binding affinity of A11 and oligomer-specific scFV antibodies to A $\beta$ <sup>65</sup>. Oppositely, aptamers of KM33 and KM41<sup>95</sup> that were found to bind to A $\beta$  fibrils could also recognize other amyloid fibrils of insulin, IAPP, lysozyme, and prion<sub>106-126</sub>, with 15–17-fold higher sensitivity compared to ThT fluorescence. In combination of charge or conformational-driving recognition capacity of aptamers, there are still a large room to design aptamers with integrated diverse functionalities for achieve the highly specific and sensitive probes for A $\beta$  detection.

### 2.3. Peptide-based probes

In comparison with widely used biorecognition elements such as antibody, aptamer, enzyme, nucleic acid, protein receptor etc., peptides have many advantages, making them ideal candidates for biosensor development. Peptides can provide the excellent affinity and specificity of an antibody; They are small in size, significantly decreasing their susceptibility to proteases and non-specific binding/trapping of antigen; They can be mass-produced through standard solid-phase synthesis protocols at low cost.

Peptide-based probes can be readily designed in a way to have similar structure and sequence to the targeted A $\beta$ . A general design principle of A $\beta$ -targeting peptides is to search similar sequence to A $\beta$  or similar characteristic  $\beta$ -sheet structure to A $\beta$  by homologues sequence and structure mapping<sup>98</sup>. Specifically, A $\beta$ -targeting peptides is derived from different fragments of full-length A $\beta$ . Since these fragmental peptides have the same sequences as their parenting A $\beta$ , they are very likely to fold into similar structure to A $\beta$  so as to recognize and bind to A $\beta$  via homologous interactions. Another design strategy of A $\beta$ -targeting peptides is inspired from the co-localization/cross-seeding between A $\beta$  and other natural proteins *in vivo*. Small peptide-A $\beta$  interactions are generally involved a wide combination of electrostatic forces, hydrogen bonds, hydrophobic interactions, and van der Waals forces. For instance, based on the cross-seeding interactions, a hIAPP<sub>8-18</sub> fragment exhibited strong binding to A $\beta_{40}$  with 275 nM binding affinity<sup>68</sup>. Further studies have also identified different peptides to bind to A $\beta$ . The rPK-4 polypeptide, homologous to PCM-1 protein (interacting with A $\beta$  *in vivo*), was found to bind A $\beta_{42}$  oligomers with nanomolar affinity via its binding sequence

(KDKTPKSKSK) located at the N-terminal<sup>67,99</sup>.

Another new design strategy for peptide-based A $\beta$  probes is to derive from peptide-based amyloid inhibitors, because both “inhibition” and “detection” of A $\beta$  aggregates requires the strong interactions to be occurred between inhibitors/detectors and A $\beta$ . Many peptide-based inhibitors were designed from amyloid sequences. Due to sequence homology, it is not surprising to observe the binding affinity of peptide inhibitors with A $\beta$ . For instance, most of peptide-based A $\beta$  inhibitors were derived from the central hydrophobic sequence A $\beta$ <sub>16-20</sub> (KLVFF) and C-terminal fragment A $\beta$ <sub>39-42</sub> (VVIA)<sup>100, 101</sup>. To further improve binding affinity to A $\beta$ , two positively charged residues (R, K) were incorporated into LVFFA, which significantly promoted the binding to A $\beta$  via increased electrostatic interactions at the  $\beta$ -sheet region of A $\beta$ <sup>102, 103</sup>. Recently, we proposed a “like-interacts-like” hypothesis to de novo design different hexapeptides with self-assembled ability to form  $\beta$ -sheet-rich structures. These hexapeptides also demonstrated their sensing ability to interact with A $\beta$  via  $\beta$ -sheet interactions with 0.8-4.5  $\mu$ M binding affinity<sup>69</sup>.

#### 2.4. Small molecule-based probes

Apart from the above-mentioned antibodies/aptamers/peptides being extensively used as amyloid probes, small chemical molecules are another type of amyloid probe. Since these small molecule probes often contain aromatic rings, quinones, and/or acidic hydroxyl groups, the favorable binding between small molecules and A $\beta$  mainly stems from the synergistic interactions of  $\pi$ - $\pi$  stacking, hydrophobic interaction, electrostatic interaction. Specifically, small molecules including natural exists molecules (e.g. curcumin<sup>104</sup>, resvaretol<sup>105</sup>, catechin<sup>106</sup>, genistin<sup>107</sup>, tanshinone<sup>108</sup>) and synthetic molecules (e.g. Congo red<sup>109</sup>, indoles<sup>110</sup>, melatonin<sup>111</sup>) particularly target the structurally characteristic regions containing hydrophobic grooves,  $\beta$ -sheet structure, planar structure, shape complementation, and aromatic/basic/acidic residues of A $\beta$  aggregates. Small molecule are workable for probing different A $\beta$  aggregates, i.e. A $\beta$  monomers, oligomers, (proto)fibrils, and plaques<sup>26, 30, 110</sup>.

In addition to strong binding ability, some small molecules are fluorescent molecules (e.g. ThT<sup>39</sup>, ThS<sup>112</sup>, congo red<sup>113</sup>, ANS<sup>26</sup>), which also possess a self-emission property to display fluorescence upon binding to A $\beta$ , allowing for directly probing and visualizing simultaneously. These fluorescent molecules consist of a  $\pi$ -conjugated system end-capped with strong donor and acceptor moieties (donor- $\pi$ -acceptor). The binding between fluorescent molecules and A $\beta$  will causes conformational changes, restrict molecular motion, or induce Förster resonance energy transfer (FRET) changes, all of which trigger fluorescence emission along with a shift of the maximum emission wavelength  $\lambda_{max}$  in the emission spectra. For another type of small fluorescence molecules (e.g. Cur-N-BF<sub>2</sub><sup>36</sup>, TPE derivatives<sup>114</sup>, PD-NA<sup>115</sup>) capable for binding to A $\beta$  and turning on fluorescence signals, they mostly contain molecular rotors (e.g. rotatable aromatic rings). Once they bind to A $\beta$ , the intermolecular interactions between small molecules and A $\beta$  aggregates will restrict the rotation of the rotors, which consume

excited-state energy through the rotation of the aromatic rotors, thus leading small molecules to decay via radiative channels. Taking advantage of the binding between A $\beta$  and small molecules, surface plasmon resonance (SPR)<sup>116</sup> and quartz crystal microbalance (QCM)<sup>117</sup> have been utilized for the qualitative and quantitative detection of A $\beta$  formation. Finally, from amyloid inhibition viewpoint, these small molecule probes have also been reported to possess the inhibition ability to prevent amyloid aggregation and even disassemble the preformed amyloid fibrils<sup>104, 107, 108, 118</sup>.

### 3. Sensing Materials and Biosensors for A $\beta$ Detection

Currently, there is still no any definitive biosensor used for AD diagnostics, because the precise AD-related biomarkers are not completely identified for diagnosis and response-monitoring. Despite of many invariably fails so far for AD diagnostics, tremendous attempts have also established different sensing strategies, designed different probes, and fabricated different biosensors for A $\beta$  detection with improved sensitivity and specificity at sub-stoichiometric concentrations. Among various biosensor systems for A $\beta$  detection, four types of the biosensors of fluorescent imaging sensors, electrochemical sensors, surface-enhanced Raman scattering biosensors, and colorimetric sensors stand out because of their high sensitivity and specificity, briefness, efficiency, and easy configuration.

First, “seeing is believing”, so the most convincing diagnostic strategy is to develop different imaging approaches for targeting different AD biomarkers. Considering that the existence of A $\beta$  plaques and tau tangles is compelling evidence in the biopsy sampling and staining of AD brain tissues, different imaging techniques and agents, including positron emission tomography (PET) imaging, single-photon emission computed tomography (SPECT), and magnetic resonance imaging (MRI), have been developed to detect and image A $\beta$  plaques and/or tau tangles<sup>119</sup>, based on distinct A $\beta$  or tau pathology hypothesis. Moreover, small fluorescent molecules (e.g. thioflavin T, Congo Red, Pittsburgh compound B, aggregation-induced emission molecules) have been developed to detect A $\beta$ -based biomarkers for ex vivo and in vivo imaging due to their multiple advantages of strong blood–brain barrier (BBB) permeability, specific targeting of  $\beta$ -structure-rich A $\beta$  aggregates, and fast clearance kinetics. Generally, these fluorescent molecules contain several aromatic rings in a small and planar structure and possess the longer wavelength excited states near the far-red or NIR regions. Such structural features enable them to interact with similar aromatic or planar residues in the  $\beta$ -sheet regions of A $\beta$  aggregates via  $\pi$ - $\pi$  stacking and hydrophobic interaction, with possible additional binding affinity of hydrogen bondings in some cases. Strong binding affinity of fluorescent molecules to A $\beta$  aggregates will induce restricted rotational motion of fluorescent molecules in a local congested environment and trigger their intramolecular charge transfer (ICT) states, leading to enhanced fluorescence emission at the deep tissue regions. Probes with a flexible  $\pi$ -conjugated backbone offers strong fluorescence enhancement with minimized background signal when they bind to A $\beta$ .

Second, colorimetric sensors are mainly built on stimuli-responsive colorimetric materials, which offer the easy and convenient detection of A $\beta$  in response to external stimuli. Most of colorimetric sensors employ gold nanoparticles (AuNPs) as sensing elements due to their unique surface plasmon resonance effect. To improve better detection sensitivity and selectivity of A $\beta$ , AuNPs are often functionalized with designed ligands (e.g. antibodies<sup>120</sup>, enzymes<sup>121</sup>, aptamer<sup>122</sup>, zeolitic frameworks<sup>20</sup>, and peptides<sup>64</sup>) to create specific nanoprobcs with strong binding affinity to A $\beta$ . On the other hand, the size of nanoparticles and the nanoparticle-coated ligand interactions also strongly affect sensor performance.

Third, electrochemical and biochemical sensors are another typical diagnostic approach<sup>123, 124</sup>. A general working principle of electrochemical biosensor for A $\beta$  detection is based on (i) specific electron-transfer reactions between electroactive residues (Tyr10, His6, His13, His14, and Met35) and designed receptors (e.g., antibody, binding agents), (ii) A $\beta$ -induced metal ion homeostasis (Ca<sup>2+</sup>, Zn<sup>2+</sup>, Cu<sup>2+</sup>). Since metal ions often bind to A $\beta$  and consequently modify A $\beta$  aggregation pathways, novel ion selective electrodes (ISEs) are typically used as the sensing platform to ensure specific selectivity ions of interest. Chemical signals resulted from probe-A $\beta$  binding will be converted to detectable electronic signals via an electrochemical transducer (e.g., an electrode or field-effect transistor).

Four, advanced spectroscopic techniques, such as infrared and Raman spectroscopy, offer high sensitivity (pM detection limit) and inherent selectivity to detect A $\beta$  aggregates, but they also limited by complex instrumentation and additional reagents being introduced to the sample milieu. Different from other biosensors that only detect one targeting biomarker at a time, spectroscopic sensors can simultaneously distinguish a range of different biomarkers in a complex sample (e.g. tissue, CSF, blood) via “spectral fingerprint” peaks. Almost all of the above-mentioned biosensors are still limited to mature A $\beta$  (proto)fibrils or plaques or to the validation of dementia symptoms at the very late stage, and early A $\beta$ -oligomer-targeting diagnosis is still not convincingly established. Thus, the early and accurate of A $\beta$  detection is critical for both AD diagnostics and AD treatment before significant brain damage and neuronal loss become irreversible.

### 3.1. Fluorescent imaging sensors

Fluorescent imaging sensors are considered as the most reliable diagnostic tool to distinguish AD patients from normal controls by in vivo detecting A $\beta$  plaques in human brains for monitoring the neurodegenerative progress of AD. To achieve this goal, a combination of clinically useful fluorescent probes (e.g. <sup>11</sup>C-PiB<sup>125</sup>, <sup>18</sup>F-Flutemetamol<sup>126, 127</sup>, <sup>18</sup>F-Florbetaben<sup>128</sup>, and <sup>18</sup>F-Florbetapir<sup>129, 130</sup>) and novel imaging techniques (e.g. positron emission tomography (PET), single-photon emission computed tomography (SPECT), and magnetic resonance imaging (MRI)) has been developed for clinical use with color image readings to facilitate AD diagnosis. However, these neuroimaging sensors mainly target A $\beta$  plaques, which are

questionable about their serving as major neurodegeneration biomarkers. Technically, *in vivo* A $\beta$  probes to achieve high resolution imaging also require high quantum yield upon binding, near-infrared (NIR) emission wavelength beyond the background tissue auto-fluorescence range (ideally between 650 nm and 900 nm), high metabolic stability, high blood-brain barrier (BBB) permeability, low toxicity, and fast brain uptake and washout kinetics, all of which add up to major technical hurdles and motivate efforts to develop alternative imaging sensors.

*Ex vivo* optimal images offer more diverse and relatively convenient ways to analyze A $\beta$  samples collected from the brain slices, CSF, and blood at different disease stages with high-resolution images both *in vivo* and *in vitro*. The first fluorescent thioflavin-T (ThT) probe used for amyloid detection was traced back to 1959<sup>39</sup>. Since then, ThT is the most commonly used fluorescence chemicals for amyloid fibril detection (not limited to A $\beta$ ). ThT is planar molecular and contains both electron acceptor (benzothiazole) and donor (aniline), allowing it to freely rotate around the C-C bond at unbound state. But, ThT favors to bind to the hydrophobic  $\beta$ -sheet grooves of A $\beta$  aggregate with binding affinity of 580 nM<sup>125</sup>, which would restrict the motion of ThT and suppress fluorescence quenching, leading to red-shift in fluorescence emission maxima from 440 nm (excitation at 350 nm) to 482 nm (excitation at 450 nm)<sup>131</sup>.

Following the similar binding-induced fluorescence mechanism, many probes (e.g. PiB, BODIPY derivatives, CRANAD derivatives, and DANIRs) have been designed and discovered to show high binding selectivity and affinity to the hydrophobic grooves on the  $\beta$ -sheet surface along A $\beta$  fibril axis and to exhibit a variety of responses to amyloids, such as intensity changes, shifts in fluorescence maxima, and variations in lifetimes (**Figure 3**). For example, PiB as a ThT analogue is designed to improve the penetration and clearance in the brain through the structural modification for increasing lipophilicity/hydrophobicity and making electrostatic neutral<sup>40</sup>. Similar to PiB, another series of benzothiazole Schiff-bases, a combination of pharmacophore structure of PiB (i.e. benzothiazole and phenyl group) and C=N as linker, were synthesized to improve binding affinity to f-A $\beta$  up to 4.38 nM<sup>132</sup>. To achieve long wavelength emission, properly electronic structure is required on the basis of the similar push-pull architecture to ThT, e.g. suitable donor and acceptor pair with a smaller HOMO-LUMO gap, interconnected by highly polarizable  $\pi$ -conjugated bridge are expected to emit fluorescence in NIR region. NIAD-4<sup>41</sup>, as a A $\beta$  plaque-targeting NIR probe, possesses a donor group (p-hydroxyphenyl) and a acceptor group (dicyanomethylene) connected by dithienylethenyl  $\pi$ -bridge. NIAD-4 can cross BBB to bind to A $\beta$  aggregates, and upon its binding, NIAD-4 emits strong fluorescence of >600 nm with a striking 400-fold signal enhancement, leading to high binding affinity (10 nM) *in vivo*. Other classical NIR probes with the donor-acceptor architecture include boron dipyrromethane (BODIPY) based fluorescence molecules<sup>22</sup> (e.g. BODIPY<sup>742</sup>, BAP-1<sup>44</sup>, Aza-BODIPY<sup>133</sup>, BD-Oligo<sup>49</sup>) with high quantum yield, BBB-penetrating curcumin derivatives (e.g. CRANAD-2<sup>45</sup>, CRANAD-3<sup>134</sup>, CRANAD-58<sup>24</sup>), DANIRs<sup>43</sup>, styryl-based probe<sup>46</sup>, and IRI-1 probe<sup>19</sup>, all of which exhibit a high specificity toward A $\beta$



plaques with high binding affinity of 27-380 nM *in vivo*, not tau or  $\alpha$ -synuclein fibrils<sup>135</sup>.

Different from these above-mentioned fluorophores that may suffer from aggregation-caused self-quenching (ACQ) at A $\beta$  aggregate sites, aggregation-induced emission fluorogens (AIEgens) feature several advantages for detecting protein aggregates, including lower background, higher signal-to-noise ratio and sensitivity, better accuracy, and more outstanding resistance to photobleaching<sup>35</sup>. AIEgens recently have been used as amyloid probes to monitor the fibrillation process of different amyloid proteins. A general working principle of AIEgens lies on the fact that upon AIEgens to the hydrophobic  $\beta$ -sheet-structures of A $\beta$  aggregates, aggregation-induced restriction of intramolecular rotations, transition, and/or vibration turns on the charge transition from a local excited state to the intramolecular charge transfer state, initiating fluorescence emission. The 1,2-bis[4-(3-sulfonatopropoxy)phenyl]-1,2-diphenylethene sodium salt (BSPOTPE) was the first iconic AIE luminogen and used to monitor insulin aggregation *ex situ* ( $\lambda_{ex}$  = 350 nm,  $\lambda_{em}$  = 480 nm) and to suppress the insulin fibrillation at very low dose<sup>23</sup>. Later, tetraphenylethene tethered with triphenylphosphonium (TPE-TPP), was synthesized and used to probe  $\alpha$ -synuclein with a much high signal-to-noise ratio than ThT<sup>47</sup>. Apart from the AIEgens for the amyloid fibrillation detection and monitoring in solution, AIEgens can also work in living tissues and cells in AD brain by conjugating with peptides/proteins, DNA/RNA, carbohydrates, and nanoparticles to facilitate BBB permeation, enhance NIR wavelength range, and to maintain the fluorescence-off state before binding to A $\beta$  deposition<sup>136</sup>. To obtain superior spatiotemporal resolution, a series of AIE-active molecules were designed and synthesized with nearly planar donor-acceptor structures. Unlike traditional AIEgens, since the planar-like structure of AIE-active molecules facilitate the molecular insertion into the  $\beta$ -sheet structure of f-A $\beta$ , AIE-active molecules can image A $\beta$  plaques in the brain slices of Tg mouse *ex-vivo* with  $\sim$ 30 nm optical resolution<sup>115</sup>. Another AIEgen example is QM-FN-SO<sub>3</sub>, which was rationally designed by introducing lipophilic  $\pi$ -conjugated thiophene-bridge to extend the fluorescence emission wavelength to a NIR region at 720 nm, with the higher binding affinity (compared with ThT) to A $\beta$  plaques in AD-model mice.<sup>48</sup>

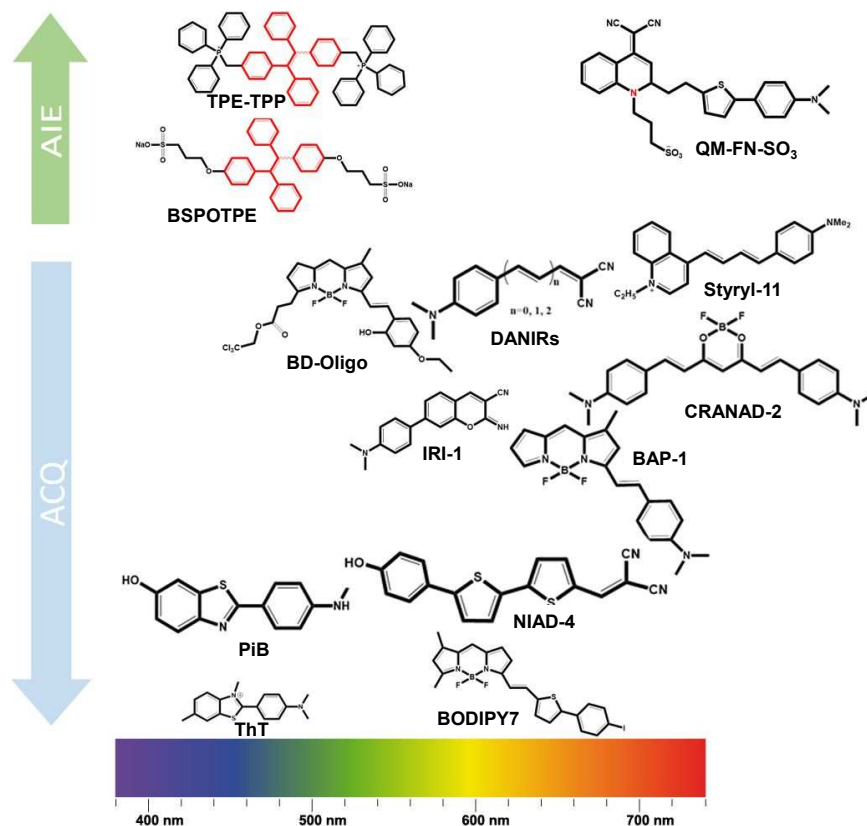


**Figure 3.** Two typical ACQ- and AIE-based fluorescent probes for A $\beta$  detection. Higher binding affinity is correlated with larger molecular size of these probes for eye guidance, with an identified emission wavelength range for each probe.

Apart from insoluble amyloid plaques in brain, soluble A $\beta$  oligomeric aggregates are considered as the most neurotoxic intermediates, which exist in CSF and plasma and are more biologically relevant to the neurodegeneration of AD<sup>137</sup>. Thus, A $\beta$  oligomer-targeting probes in CSF or blood samples are more beneficial for clinical diagnosis. BODIPY-Oligomer (BD-Oligo)<sup>49</sup>, as the first designed oligomer-specific fluorescent probe, responded strongly ( $K_d = 480$  nM) to A $\beta$  oligomers at  $\lambda_{em} = 530$  nm. The BODIPY ring and the phenyl ring are recognized by hydrophobic F19/V36 residues, and the carbonyl group of BD-Oligo forms CH-O bonding with V36 residue in oligomeric A $\beta$ . Intraperitoneal injection of BD-Oligo into Tg mouse allowed it to penetrate across BBB and present fluorescent labeling of brain tissues without observable toxicity. Moreover, due to metal ion chelation with A $\beta$ , ratiometric BPNS probe was designed to capture a complex of Zn<sup>2+</sup>-bound A $\beta$  oligomer in diluted blood serum<sup>21</sup>. While several studies<sup>24, 133, 134, 138-140</sup> have reported that fluorescent amyloid probes can bind to both oligomeric and fibrillary amyloids with different binding affinity and distinguish them with different fluorescence intensities, major efforts are still needed to develop fluorescent-based probes to strongly discriminate oligomeric A $\beta$  from fibrillar A $\beta$ .

### 3.2. Electrochemical A $\beta$ sensors

Different from neuroimaging techniques for A $\beta$  detection that require sophisticated instruments, tedious clinical process, expensive labels, and highly skilled researchers, electrochemical A $\beta$  sensors are simple, rapid, inexpensive, and label-free techniques for the detection of A $\beta$  aggregation. A number of electrochemical A $\beta$  sensors have been developed for detecting A $\beta$  species, its aggregation kinetics, and interactions with drugs, antibodies, and metal ions in aqueous solutions, cell-derived samples, CSF, and blood<sup>141-144</sup>. A general sensing principle is relied on the specific and high affinity interaction between electrodes and A $\beta$ , but from a targeting viewpoint of A $\beta$ , most of electrochemical sensors are designed to target the electroactive residues of Tyr, His, Met in A $\beta$  via redox oxidation. Since A $\beta$  contains one Tyr, Met and three His, the adsorption-induced oxidation of these residues of A $\beta$  on electrodes allows to trigger the intermolecular electron transfer rate of redox reactions and the rise of oxidation current peaks (**Figure 4a**)<sup>145, 146</sup>. However, A $\beta$  misfolding and aggregation often affects the proximity of Tyr, His, Met to the transducing electrode; leading to the reduction in the oxidation signals. This poor signal transductivity would become even more pronounced in blood and CSF samples where nonspecific protein adsorption (e.g. albumin, globulin, fibrinogen) on the electrodes will further interfere with electrochemical signals (i.e. oxidation current) as produced by the specific A $\beta$ -probe interactions. To overcome such poor selectivity, different chemical-to-electrical signal amplification strategies have been proposed and implemented to improve their detection sensitivity and limit, including (i) the coating of a combination of nanocomposites (e.g. nanoparticles, metal-organic frameworks, carbon-based materials) and probes (e.g. peptides, enzymes, antibodies) onto electrodes, where the former to increase electronic conductivity and the latter to enhance signal-to-noise ratios and (ii) the development of multilayer or sandwich structures on electrodes to enhance the electronic transmission capability between electrode surfaces and A $\beta$ <sup>147</sup>. Apart from sensing materials, use of different methods for electrochemical signal analysis also impacts the detection limit of A $\beta$ , including voltammetry (e.g. square wave voltammetry, SWV<sup>141</sup>; differential pulse voltammetry, DPV<sup>148, 149</sup>; linear-sweep voltammetry, LSV<sup>58</sup>; and cyclic voltammetry, CV<sup>150, 151</sup>), electrochemical impedance spectroscopy (EIS)<sup>152</sup>, and electrochemiluminescence assay (ECL)<sup>50</sup>.

Based on the above mentioned design principles, a number of different biosensors were developed for detecting different species of A $\beta$  ranging from monomers, oligomers, to fibrils/plaques by coating the electrodes with fluorescence molecules, nanoparticles, peptides, and antibodies to expand detection limits and signal amplification via redox cycling, enzymatic catalysis, and plasmonic effects between electrodes and A $\beta$ <sup>153-156</sup>. Among them, the most straightforward electrochemical sensors for A $\beta$  detection is to coat fluorescence molecules (e.g. ThT and Congo red) on the electrodes and used them as recognition motifs to interact with the  $\beta$ -sheet structure of A $\beta$  so as to generate anodic oxidation signals for detection<sup>157, 158</sup>. A nanostructured isoporous membrane<sup>57</sup> of block copolymer poly(styrene-*b*-4-vinylpyridine) was functionalized with Congo red (CR) probes, followed by the placement of CR-coated

membrane on PEDOT:PSS channels, thus producing a micron-scale organic electrochemical transistor (OECT)-based membrane microchannel sensor with a channel width of 100  $\mu\text{m}$  and a channel length of 10  $\mu\text{m}$  (**Figure 4b**). The resultant OECT membrane sensors showed specific recognition and interactions with A $\beta$  aggregates via membrane-coated CR in human blood serum, with A $\beta$  detection limit of 221 nM.

Uses of metals NPs to modify the electrodes become another common strategy to develop NP-based electrochemical sensors for A $\beta$  detection with enhanced electrical conductivity. A very simple electrochemical sensor was developed by the coating of gold nanoparticles (Au NPs) of different sizes on the indium tin oxide (ITO) electrode in the presence of antifouling polyethylene glycol (PEG) as surfactant agents. The resultant AuNPs/ITO sensors achieved a significantly redox signal enhancement and the low detection limit of 50 nM for A $\beta$  in PBS<sup>159</sup>. But due to lack of specific binding between AuNPs and A $\beta$ , this sensor is very unlikely to be worked in the mixed or complex media (e.g. multiple protein solution, blood serum, CSF).

Several peptide-based electrochemical biosensors were also developed by immobilizing (i) cysteine-containing PrP<sub>95-110</sub> peptide<sup>150</sup>, (ii) ferrocene (Fc)-labeled MUA-RGTWEGKWK<sup>160</sup> and KLVFF peptides<sup>17</sup>, and (iii) cucurbituril<sup>161</sup> onto a gold electrode for the capture of A $\beta$  oligomers from several blood serum samples, with a detection limit of 3 pM, 240 pM, and 48 pM, respectively. While all electrode-coated peptides have a completely different recognition sequences, they both contain aromatic residues for recognizing and binding to A $\beta$  oligomers via hydrophobic interaction and  $\pi$ - $\pi$  stacking.

Due to the non-redox nature of antibody-A $\beta$  interactions, antibody-based electrochemical biosensors were developed to detect A $\beta$  species using antibody-modified electrodes<sup>153, 162</sup>. Since the mAb is well known to have a selectively binding to the common N-terminus of all A $\beta$  species, mAb-modified sensors exhibited strong selectivity and specificity to detect A $\beta$ <sub>40</sub>, A $\beta$ <sub>42</sub> and A $\beta$ <sub>16</sub> from CSF with a detection limit of 5-10 pM. Such high selectivity is attributed to (i) the strong antibody-antigen (mAb-A $\beta$ ) interactions and (ii) the signal amplification of AuNPs to promote the oxidation current. Different from one-vs.-one antibody-A $\beta$  strategy, a triple-barrel carbon fiber microelectrode was developed by anchoring three A $\beta$ -targeting antibodies of mHJ2, mHJ7.4, and mHJ5.1 on carbon fiber microelectrodes<sup>163</sup>, where each microelectrode contain one type of A $\beta$ -targeting antibody. The triple antibody-modified microelectrode showed not only the lower detection limit of A $\beta$ <sub>40</sub> and A $\beta$ <sub>42</sub> in CSF (20 nM), but also the faster response time (7 min) than three single-antibody microelectrodes with 1000 nM of detection limit and 6-hours of response time.

To further improve detection limit of electrochemical biosensor for A $\beta$  detection, a more common strategy is to combine multiple signal amplification methods<sup>153</sup> by using ALP-based p-aminophenol (p-AP) redox cycling to increase in the anodic current and

mAb antibody-covered electrodes to improve specific mAb-A $\beta$  interactions. Both effects promoted a detection limit to 5 pM for A $\beta$ <sub>42</sub> and total A $\beta$  from artificial CSF. Similarly, another electrochemical electrodes (**Figure 4c**), modified by three conjugated components: silver nanoparticles (AgNPs) as the redox reporters, PrP<sup>95-110</sup> as specific A $\beta$  oligomer-binding peptide, and  $\beta$ -cyclodextrin ( $\beta$ -CD) as electrochemical signal amplifier, were developed to show highly specific detection for A $\beta$  oligomer with a detection limit of 8 pM, but no response to A $\beta$  monomers and fibrils<sup>58</sup>. An integration of curcumin and Ni on electrodes allowed to promote ion charge transfer and electron transport via the redox reaction between porous Ni-foam and electroactive residues in A $\beta$ , while still maintaining specific binding of curcumin to A $\beta$  oligomers via through hydrophobic interactions between at the hydrophobic phenyl and methoxyl groups of curcumin and the nonpolar regions of the A $\beta$  oligomers<sup>56</sup>, leading to the detection limit of A $\beta$  oligomers at a range of 1 pM to 10 nM in artificial CSF (**Figure 4d**).

Furthermore, it is more challenging and promising to develop electrochemiluminescence (ECL) sensors for A $\beta$  detection, an ideal integration of both electrochemical and luminescent materials into a combined electrochemical and spectroscopic electrode. As a proof-of-concept example, the “light switch” [Ru(phen)<sub>2</sub>dppz]<sup>2+</sup> molecules were introduced into a paper-based bipolar electrode (**Figure 4e**). The light-switch [Ru(phen)<sub>2</sub>dppz]<sup>2+</sup> molecule showed no ECL in aqueous solution, but exhibited strong ECL when binding to as low as 100 pM of in PBS solution, as well as detectable signals from CSFs of APP/PS1 transgenic AD model mice. Another complex example of ECL sensors was designed by first preparing a hybrid dimethyl diallyl ammonium chloride (PDDA)/MnCO<sub>3</sub>/AuNPs platform, followed by the anchoring of HWRGWVC (HC-7) antibody on (PDDA)/MnCO<sub>3</sub>/AuNPs for A $\beta$  detection<sup>51</sup>, where MnCO<sub>3</sub> nanospheres were used as ECL emitter, AuNPs as promotor for electrical conductivity, and HC-7 as specific binding acceptor for A $\beta$  (**Figure 4f**). The resultant MnCO<sub>3</sub>/PDDA/Au/HC-7 ECL sensors enabled to achieve the ultralow detection limit of A $\beta$  at 19.95 fg/mL in human CSF.

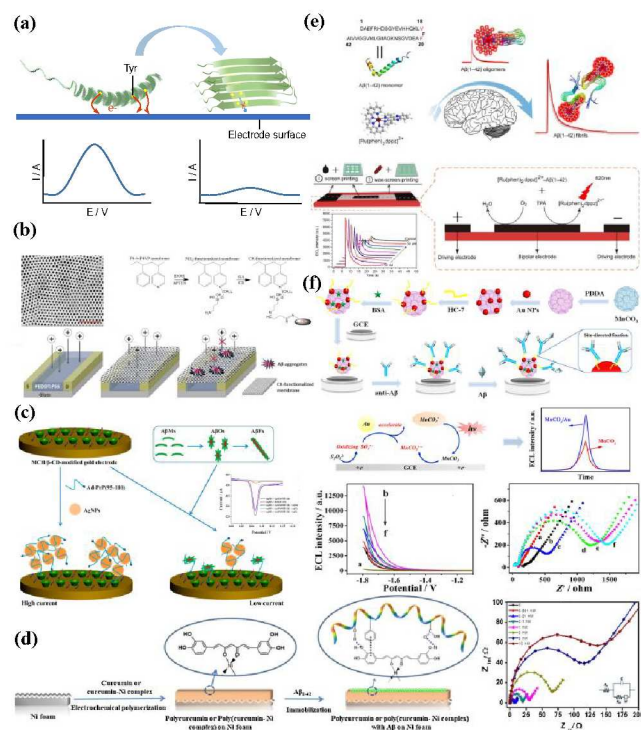


**Figure 4.** Electrochemical sensors for A $\beta$  amyloid detection. (a) Electroactive amino acids in A $\beta$  as electrochemical marker for A $\beta$  detection through voltammetry. (b) Micron-scale organic electrochemical transistor configured with CR-functionalized isoporous membrane and PEDOT:PSS channels for A $\beta$  aggregates detection. (Reprinted with permission<sup>57</sup>, copyright 2019 Elsevier) (c) PrP<sup>95-110</sup>/ $\beta$ -CD/AgNPs electrochemical sensor for selective A $\beta$  oligomers detection by the A $\beta$  oligomer-specific PrP<sup>95-110</sup> receptor. (Reprinted with permission<sup>58</sup>, copyright 2016 American Chemical Society) (d) Poly(curcumin-Ni) sensor for the detection of A $\beta$  oligomers. (Reprinted with permission<sup>56</sup>, copyright 2018 Elsevier) (e) Paper-based bipolar electrode ECL sensor using [Ru(phen)<sub>2</sub>dppz]<sup>2+</sup> as receptor for A $\beta$  detection. (Reprinted with permission<sup>164</sup>, copyright 2018 Ivyspring International Publisher) (f) ECL immunosensor based on MnCO<sub>3</sub> nanospheres for A $\beta$  detection. (Reprinted with permission<sup>51</sup>, copyright 2019 American Chemical Society)

### 3.3. Surface-enhanced Raman scattering biosensors

Surface-enhanced Raman scattering (SERS) spectroscopy has emerged as a powerful analytical technique for molecular detection at trace concentrations. The large electromagnetic fields at a well-patterned nanometal surface would give rise to strong enhancement of Raman signals as high as  $10^{10}$ - $10^{11}$  upon binding of probes to analytes and excitation with light of appropriate energy (**Figure 5a**)<sup>165</sup>, so SERS can even achieve single molecule detection<sup>166</sup>.

In the design of SERS-based amyloid detection, plasmonic AuNPs or AgNPs are often used to form a patterned surface for Raman scattering enhancement. A typical and simple example is to modify a monolayer of nanoshells with sialic acid for

specifically binding to A $\beta$ , followed by the use of Congo red to quantify the SERS signals for determining the surface amount of nanoshell-bound A $\beta$ <sup>59</sup>. A linear correlation between SERS signals and A $\beta$  concentrations reveals a detection range of A $\beta$  between 1 pM and 10 nM. Later, an improved SERS sensor was developed by conjugating Rose Bengal (RB) dye on AuNPs, in which RB is used to emit fluorescent signal, report SERS spectrum, and bind to A $\beta$  simultaneously (**Figure 5b**)<sup>62</sup>. RB-AuNPs conjugation significantly enhanced Raman signals, while the interaction between RB-AuNPs and A $\beta$  induced a remarkable enhancement in fluorescence emission. The RB-AuNPs were used for both SERS-based detection of A $\beta$ <sub>42</sub> peptides and fluorescence-based imaging of amyloid plaques, both of which contributes to the detection limit of  $\sim 0.25$   $\mu$ M, but its detection sensitivity was still needed to be improved. Apart from the use of amyloid dyes as bio-selective receptor in SERS-based biosensors, a sandwiched immunosensor consisting of silver nanogap shells (AgNGSs) and A $\beta$ -targeting antibody of CA $\beta$  on magnetic beads (CA $\beta$ -MB) was able to A $\beta$ <sub>40</sub> and A $\beta$ <sub>42</sub> in human serum based on  $\sim 10^7$  enhancement of SERS signals from the bound AgNGSs, which led to the detection limits as low as 0.25 pg/mL (**Figure 5c**)<sup>60</sup>.

Different from the use of bare AuNPs, dye-coated, and antibody-coated AgNPs for A $\beta$  detection, an aptamer-based SENS sensor, i.e. Raman dye-coded polyA aptamer-AuNPs (PAapt-AuNPs), was also developed (**Figure 5d**)<sup>61</sup>. This strategy relies on the fast and strong DNA-AuNP conjugation, in which polyA block oligonucleotides serve the two roles in anchoring onto the surfaces of AuNPs and containing antitarget aptamer for A $\beta$  detection. Upon specific binding of aptamer to A $\beta$ , such binding induced the detachment of polyA block oligonucleotides from AuNPs, thus turning on plasmonic coupling effect between adjacent AuNPs for A $\beta$  detection. This SERS assay can achieve a fast and sufficient detection of both A $\beta$ <sub>42</sub> oligomers and Tau protein simultaneously in CSF at a detection limit of  $3.7 \times 10^{-2}$  nM and  $4.2 \times 10^{-4}$  pM, respectively.

Despite of the innate ultra-sensitivity of SERS spectroscopy, the conventional SERS-based biosensors require two or multiple materials/components to serve as chemical reporter and bio-selective receptor, so the undesired vibrational spectra from diverse interference is considered as inherent limits that affect the accuracy of SERS spectra. Most SERS sensors rely on the sandwich reaction between plasmonic surface (metal NPs), Raman reporter (FC, p-MBA, and DTNB), and bio-selective receptor (A $\beta$  probe), which requires process-tedious, time-consuming, labor-intensive fabrication steps. Additional drawback of conventional SERS sensors is to use wash and separation steps to collect target-specific SERS tags for determining detection efficiency, instead to directly generates a specific SERS signal from SERS-tag-A $\beta$  (not limited to A $\beta$ ) interactions. Thus, the construction of rapid, convenient, and cost-effective multiplexed SERS assay methods is crucial to investigate the early detection of A $\beta$  and the diagnosis of AD.

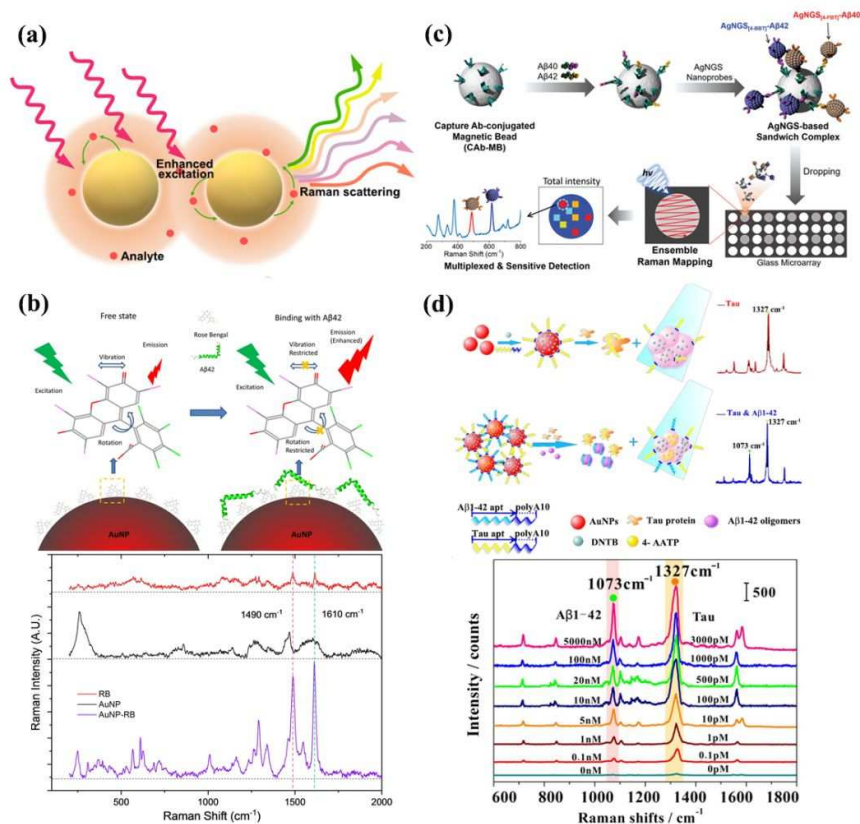


**Figure 5.** Surface-enhanced Raman scattering biosensing platform for A $\beta$  detection. (a) Mechanistic illustration of Raman signal enhancement on nanometal surfaces upon binding of analyte molecules. (b) Rose Bengal-conjugated AuNPs to achieve dual SERS/fluorescence signal enhancement for A $\beta$  detection. (Reprinted with permission<sup>62</sup>, copyright 2019 Springer Nature) (c) AgNGS sandwich nanoprobe for the detection of A $\beta$ <sub>40</sub> and A $\beta$ <sub>42</sub>. (Reprinted with permission<sup>60</sup>, copyright 2019 John Wiley & Sons) (d) PA-apptamer/Dye/AuNPs conjugates based multiplexed SERS sensor for simultaneous detection of A $\beta$  oligomers and Tau proteins. (Reprinted with permission<sup>61</sup>, copyright 2019 American Chemical Society)

### 3.4. Colorimetric A $\beta$ sensors

The abovementioned A $\beta$  sensors, including fluorescent probes, electrochemical probes, and SERS platforms, all require additional equipment for signal read-out and analysis. Differently, colorimetric sensor is more attractive for preliminary tests due to its simple operation, high sensitivity, low cost, and quick read-out by naked eyes<sup>167</sup>. Take advantage of the visible color change from interparticle plasmon coupling during the aggregation or re-dispersion of AuNPs, AuNPs have been long used as colorimetric agents for detection of small molecules<sup>168, 169</sup>, nucleic acid<sup>170</sup> and proteins<sup>171</sup>. In principle, the well-dispersed AuNPs with the diameter of 10-50 nm display red color in solution, but once AuNPs start to aggregate, the solution will slowly change its color to blue due to the surface plasmon absorption-induced red shift effect.



Colorimetric strategies for A $\beta$  detection require the careful control on the aggregation of AuNPs for achieving both high selectivity and sensitivity. Generally speaking, controlling AuNPs aggregation in the presence of A $\beta$  requires the selective binding between A $\beta$  and AuNPs, as well as stabilizing forces to retain A $\beta$ -AuNPs complexes. As a typical strategy to address A $\beta$ -induced AuNPs aggregation, AuNPs conjugated with A $\beta$ <sub>42</sub> C-terminal antibody and N-terminal antibody (C-Ab<sub>42</sub>-AuNP and N-Ab<sub>42</sub>-AuNP) allowed to specifically bind the C- and N-terminal of A $\beta$ <sub>42</sub> with the lowest detection limit of 2.3 nM<sup>172</sup>. In the presence of equal amounts of C-Ab<sub>42</sub>-AuNP and N-Ab<sub>42</sub>-AuNP, a very small amount of A $\beta$  will induce AuNPs aggregation by binding C-Ab<sub>42</sub>-AuNP and N-Ab<sub>42</sub>-AuNP to the C- and N-terminals of A $\beta$ <sub>42</sub>, accompanied with color change from red to blue in a detection range of 2.3–300 nM. This strategy can further apply to detect A $\beta$  from diluted human serum (20%) at a detection range of 50–350 nM (**Figure 6a**). A dual-functionalized AuNP was designed by covalently linking both Cu<sup>2+</sup> and hemin onto the same polyethyleneimine (PEI)-modified AuNP surface to probe A $\beta$ <sup>173</sup>, on the basis of distinct strong binding of organic compound heme (ferriprotoporphyrin IX) to A $\beta$  and inorganic Cu<sup>2+</sup> to the histidine residues and the N-terminus of A $\beta$ . The resultant PEI/AuNP–Cu–hemin probe displayed a visible color change from red to blue in response to the binding of A $\beta$ <sub>42</sub> monomers in a wide range of 0.2–5000 ng/ml, with a detection limit of 40 pg/ml (**Figure 6b**).

To avoid the tedious surface modification of AuNPs, another colorimetric sensor composed of AuNPs and freely dissolved A $\beta$  binding component (e.g. Cu<sup>2+</sup>, PrP<sup>95–110</sup>) was developed to achieve the colorimetric detection of A $\beta$  at optimal conditions (i.e. pH and binding component concentrations). For example, in the colorimetric A $\beta$ <sub>40</sub> detection assay composed of AuNPs and freely dissolved Cu<sup>2+</sup> (AuNPs/Cu<sup>2+</sup>)<sup>63</sup>, along with the increase of solution acidity (pH <5), electrostatic interactions between positively charged A $\beta$ <sub>40</sub> (pI  $\approx$ 5.5) and negatively charged AuNPs contribute to the formation of stable non-covalent bindings between A $\beta$ <sub>40</sub> and AuNPs. The coexistence of Cu<sup>2+</sup> and the dispersed A $\beta$ <sub>40</sub>-binded AuNPs tended to gradually aggregate via the strong binding of Cu<sup>2+</sup> to the histidine residues and the N-terminus of A $\beta$ , leading to the visible color change from red to blue. As a result, the AuNPs/Cu<sup>2+</sup> colorimetric sensor could achieve maximal response to A $\beta$ <sub>40</sub> at pH=5, with a detection limit of 0.6 nM and a linear colorimetric-concentration relationship in the A $\beta$ <sub>40</sub> concentration range of 10.5–261.3 nM (**Figure 6c**).

Later, an AuNPs/PrP<sup>95–110</sup>/CdTe QDs sensor was developed with dual colorimetric and fluorescent detection ability toward A $\beta$  oligomers. PrP<sup>95–110</sup> derived from cellular prion protein was introduced as a main component for the colorimetric detection of A $\beta$  oligomers and the aggregation of AuNPs. CdTe quantum dots (CdTe QDs) functioned as fluorescent indicator, which emit fluorescent signals but will be strongly quenched in the presence of dispersed AuNPs due to the inner filter effect. Initially, upon AuNPs aggregation in the presence of PrP<sup>95–110</sup>, AuNPs/PrP<sup>95–110</sup>/CdTe

QDs solution displayed blue color and strong fluorescence. However, when A $\beta$  oligomers were introduced to AuNPs/PrP<sup>95-110</sup>/CdTe QDs solution, A $\beta$  oligomers competed with AuNPs to interact with PrP<sup>95-110</sup>, which triggered the binding of A $\beta$  oligomers to PrP<sup>95-110</sup> along with the reduction of AuNPs aggregation. The re-dispersed AuNPs in response to the binding with A $\beta$  oligomers lead to the color change of bulk solution from blue to red, as well as quench the fluorescent signal of CdTe QDs simultaneously. The resultant AuNPs/PrP<sup>95-110</sup>/CdTe QDs sensor exhibit colorimetric detection limit of 0.5 nM and good linear relationship between signal and A $\beta$  oligomer concentration in the range of 1 nM to 0.5  $\mu$ M, and a fluorescent response with detection limit of 0.2 nM, and linear decrease of fluorescent signal at A $\beta$  oligomer concentration of 0.5 nM- 0.1  $\mu$ M<sup>64</sup> (Figure 6d).

Currently, colorimetric amyloid sensors are still at its infant stage, with very few proof-of-concept systems being developed for only testing pure A $\beta$  solution or a mixture solution of A $\beta$  and other proteins (e.g., BSA, IgG, or thrombin). Different factors including pH, temperature, and salts have large influence on colorimetric signals. Thus, developing a new colorimetric system in a distinguishable color range and with optical responses is highly desirable for A $\beta$  detection.

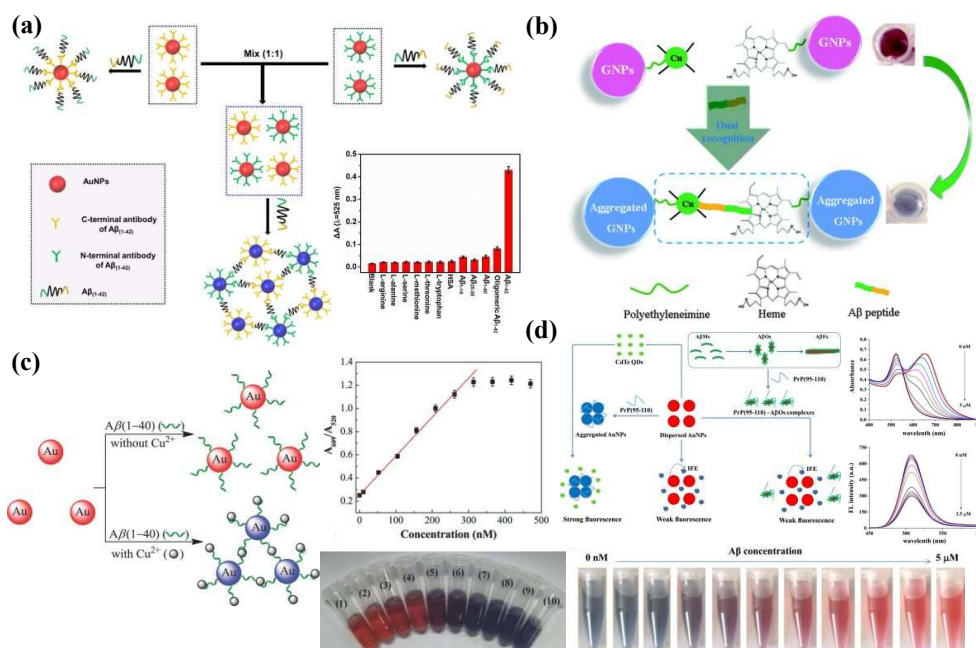


**Figure 6.** Colorimetric sensors for A $\beta$  detection. (a) AuNPs@C/N-Ab<sub>(1-42)</sub> colorimetric sandwich immunosensor for A $\beta$ <sub>42</sub> with a detection limit of 2.3 nM (Reprinted with permission<sup>172</sup>, copyright 2017 Elsevier) (b) PEI/AuNP–Cu–hemin colorimetric probe for A $\beta$ <sub>42</sub> detection with a detection limit of 40 pg/ml. (Reprinted with permission<sup>173</sup>, copyright 2015 Royal Society of Chemistry) (c) AuNPs/Cu<sup>2+</sup> colorimetric assay for A $\beta$ <sub>40</sub> detection at pH=5 with a detection limit of 0.6 nM. (Reprinted with permission<sup>63</sup>, copyright 2015 John Wiley & Sons) (d) AuNPs/PrP<sup>95-110</sup>/CdTe QDs colorimetric and fluorescent sensor for A $\beta$  oligomers with a detection limit of 0.5 nM (colorimetric detection) and 0.2 nM (fluorescent detection). (Reprinted with permission<sup>64</sup>, copyright 2016 Elsevier)

#### 4. Conclusions and Perspectives

Nowadays, while there are still no curable drugs and definitive diagnosis for AD treatment, significant progress and many clinical failures in AD treatment and diagnostics have helped to not only rule out some false or ineffective hypotheses, but also advance the understanding of the complex pathogenesis of AD, both of which will pave the pathways to major breakthroughs and final success against AD. From a diagnostic viewpoint, a major challenge for AD diagnosis is to truly identify AD-related biomarkers and underlying biological functions. AD, as a multifactorial disease, is often associated with other diseases (e.g. cardiovascular diseases, inflammatory disease, hypertension) and neurodegenerative disorders (e.g. PD and T2D). So, the mixed pathologies in these coexisting diseases make even challenging to truly identify the AD-related biomarkers. While different diagnostic and prognostic biomarkers have been proposed, none of them has achieved statistically clinical benefits and some of them even cause controversial results for investigating separate pathological pathways. These failures have prompted re-examination of the hypothesis, e.g. targeting single AD biomarker is likely not a working strategy for AD diagnostics, instead the development of multi-targeting techniques and compounds capable of simultaneously detecting several pathological biomarkers perhaps provides new strategies and solutions to undertake the complex diagnostics and pathologies of AD. It is also important to understand the pathological relationship between different biomarkers (e.g. A $\beta$ , tau, cholesterol, IgG or IgM indices, CSF:serum albumin ratio, and others<sup>13</sup>).

Second, blood- or CSF-based diagnosis, as the most emerging and promising strategy towards clinical trials, also face a great challenge for their low detection sensitivity and accuracy. Since both blood and CSF contains different AD biomarkers, current A $\beta$ -targeting probes are lack of ability to distinguish A $\beta$  from other AD-related biomarkers and AD-unrelated circulating autoantibodies/proteins in blood or CSF. Moreover, the concentration of AD biomarkers in blood or CSF are extremely low at a level of pg/ml (e.g. 25-85 pg/ml of A $\beta$  in blood and 300-420 pg/ml of A $\beta$  in CSF)<sup>13, 174</sup>, which add additional technical barriers for precise ultrasensitive detection, not to mention that the analysis of CSF is an expensive, invasive, and very painful process particularly for the elder AD patients. To realize the discrimination of A $\beta$  from other AD biomarkers or AD-unrelated substances, an in-depth understanding on the

structural details of A $\beta$  is required to improve the specificity of A $\beta$ -targeting probes. Additionally, A $\beta$  diagnostic sensitivity would be improved by combining the diagnostic strategies (e.g. trap or screen out unrelated proteins/substances) and adequate signal processing (e.g. signal amplification or background cancellation).

Third, despite the great efforts and progress in the detection of A $\beta$  protofibrils/fibrils/plaques with well-defined  $\beta$ -structures, however, it is challenging to detect amyloid oligomers. It is generally accepted that A $\beta$  oligomers are more pathologically relevant species than A $\beta$  fibrils or monomers due to their high toxicity to neuronal cells. However, since A $\beta$  oligomers are structurally disordered, unstable, and polymorphic without  $\beta$ -sheet-rich structure as a fingerprint binding motif, it remains a great challenge to design structural-based oligomer-specific probes for detecting A $\beta$  oligomers. Additionally, A $\beta$  oligomers have a broad range of structural and property variations in size, shape, solubility, charge, and hydrophobicity, making even more challenging to design a universe probe for detecting or distinguishing all or specific A $\beta$  oligomers. Design of conformation-dependent antibodies could be a feasible strategy to detect and distinguish A $\beta$  oligomers from  $\beta$ -structure-rich A $\beta$  protofibrils/fibrils because of the fundamental differences in the peptide backbone.

Fourth, from computational viewpoint, the rapid advance in artificial intelligence (AI), deep learning, and data mining provides opportunities for the discovery and development of innovative A $\beta$ -targeting probes. Quantitative structure–activity relationships (QSAR) and computational chemogenomics can be used to design different A $\beta$ -targeting probes, predict their probe–A $\beta$  interactions, and assess the sensing efficacy of the designed probes. But, a significant hurdle to discovery of A $\beta$ -targeting probes is to reconcile the inconsistent A $\beta$ -targeting probe data obtained from different labs for constructing a reliable and benchmark dataset for AI-assisted probe discovery. In addition, molecular simulation techniques (e.g. coarse-grained simulations, multiple-resolution models, enhanced sampling algorithms, and accurate atomistic force fields) are highly promising to achieve computational structure-based design of A $\beta$  probes, including the exploration and understanding of binding mechanisms between probes and A $\beta$  in different environments (e.g. aqueous solution, lipid bilayers, cell-mimic membranes), determination of binding sites, binding forces, and binding structures, and assessment of binding selectivity of the probes with respect to different A $\beta$  species.

From a different viewpoint, considering that “inhibition” and “detection” of A $\beta$  requires the strong interactions to be occurred, hypothetically all A $\beta$  inhibitors could be used as A $\beta$  detectors, and *vice versa*. High-throughput screening can be used to screen A $\beta$  inhibitor libraries to discover potential probes for A $\beta$  binding and detection. These inhibitors or probes could be mutually used for study the kinetics of amyloid aggregation, the elucidation of binding sites in amyloid structures, and the staining of amyloids aggregates *in vitro*, *ex vivo*, and *in vivo*. All challenges require a critical and complete understanding of AD from different mechanistic aspects (e.g. APP cleavage,

A $\beta$  and tau misfolding and aggregation, protein transmission between cells). Finally, increasing research funding is also a very important factor for maintaining momentum to resolve these key issues and challenges and for continuously making progress towards the effective diagnostics and therapies of AD.

**Acknowledgement.** We highly appreciate the previous financial supports from NSF grants (1510099, 1158447, and 0952624) in the past decade to move forwards our amyloid works from fundamental research to translational research.

**References:**

1. T. Niccoli and L. Partridge, *Current Biology*, 2012, **22**, R741-R752.
2. R. C. Brown, A. H. Lockwood and B. R. Sonawane, *Environmental health perspectives*, 2005, **113**, 1250-1256.
3. M. Baumgart, H. M. Snyder, M. C. Carrillo, S. Fazio, H. Kim and H. Johns, *Alzheimer's & Dementia*, 2015, **11**, 718-726.
4. N. Franzmeier, A. Rubinski, J. Neitzel, Y. Kim, A. Damm, D. L. Na, H. J. Kim, C. H. Lyoo, H. Cho and S. Finsterwalder, *Brain*, 2019, **142**, 1093-1107.
5. D. C. Perry, V. E. Sturm, M. J. Peterson, C. F. Pieper, T. Bullock, B. F. Boeve, B. L. Miller, K. M. Guskiewicz, M. S. Berger and J. H. Kramer, *Journal of neurosurgery*, 2016, **124**, 511-526.
6. X. Du, X. Wang and M. Geng, *Translational neurodegeneration*, 2018, **7**, 2.
7. J. Hardy and D. J. Selkoe, *science*, 2002, **297**, 353-356.
8. C. Janus, J. Pearson, J. McLaurin, P. M. Mathews, Y. Jiang, S. D. Schmidt, M. A. Chishti, P. Horne, D. Heslin and J. French, *Nature*, 2000, **408**, 979-982.
9. V. M. Lee, M. Goedert and J. Q. Trojanowski, *Annual review of neuroscience*, 2001, **24**, 1121-1159.
10. E. D. Roberson, K. Scarce-Levie, J. J. Palop, F. Yan, I. H. Cheng, T. Wu, H. Gerstein, G.-Q. Yu and L. Mucke, *Science*, 2007, **316**, 750-754.
11. N. L. Foster, *The Lancet Neurology*, 2007, **6**, 667-669.
12. B. Olsson, R. Lautner, U. Andreasson, A. Öhrfelt, E. Portelius, M. Bjerke, M. Hölttä, C. Rosén, C. Olsson and G. Strobel, *The Lancet Neurology*, 2016, **15**, 673-684.
13. K. Blennow, H. Hampel, M. Weiner and H. Zetterberg, *Nature Reviews Neurology*, 2010, **6**, 131-144.
14. R. S. Desikan, W. K. Thompson, D. Holland, C. P. Hess, J. B. Brewer, H. Zetterberg, K. Blennow, O. A. Andreassen, L. K. McEvoy and B. T. Hyman, *Molecular neurodegeneration*, 2013, **8**, 39.
15. T. Philips and W. Robberecht, *The Lancet Neurology*, 2011, **10**, 253-263.
16. O. Preische, S. A. Schultz, A. Apel, J. Kuhle, S. A. Kaeser, C. Barro, S. Gräber, E. Kuder-Bulletta, C. LaFougere and C. Laske, *Nature medicine*, 2019, **25**, 277-283.
17. S. Beheshti, S. Martić and H. B. Kraatz, *ChemPhysChem*, 2012, **13**, 542-548.
18. M. Chakravarthy, H. AlShamaileh, H. Huang, R. K. Tannenberg, S. Chen, S. Worrall, P. R. Dodd and R. N. Veedu, *Chemical communications*, 2018, **54**, 4593-4596.
19. J. Shin, P. Verwilst, H. Choi, S. Kang, J. Han, N. H. Kim, J. G. Choi, M. S. Oh, J. S. Hwang, D. Kim, I. Mook-Jung and J. S. Kim, *Angewandte Chemie*, 2019, **131**, 5704-5708.
20. J. Qin, M. Cho and Y. Lee, *ACS Applied Materials & Interfaces*, 2019, **11**, 11743-11748.
21. C. Li, L. Yang, Y. Han and X. Wang, *Biosensors and Bioelectronics*, 2019, **142**, 111518.
22. A. Ojida, T. Sakamoto, M.-a. Inoue, S.-h. Fujishima, G. Lippens and I. Hamachi, *Journal of the American Chemical Society*, 2009, **131**, 6543-6548.
23. Y. Hong, L. Meng, S. Chen, C. W. T. Leung, L.-T. Da, M. Faisal, D.-A. Silva, J. Liu, J. W. Y. Lam, X. Huang and B. Z. Tang, *Journal of the American Chemical Society*, 2012, **134**, 1680-1689.
24. X. Zhang, Y. Tian, Z. Li, X. Tian, H. Sun, H. Liu, A. Moore and C. Ran, *Journal of the American Chemical Society*, 2013, **135**, 16397-16409.
25. F. Shewmaker, R. P. McGlinchey and R. B. Wickner, *Journal of Biological Chemistry*, 2011, **286**, 16533-16540.
26. B. Bolognesi, J. R. Kumita, T. P. Barros, E. K. Esbjorner, L. M. Luheshi, D. C. Crowther, M. R.

- Wilson, C. M. Dobson, G. Favrin and J. J. Yerbury, *ACS chemical biology*, 2010, **5**, 735-740.
27. M. Zhang, J. Zheng, R. Nussinov and B. Ma, *Antibodies*, 2018, **7**, 25.
28. M. Zhang, B. Ren, H. Chen, Y. Sun, J. Ma, B. Jiang and J. Zheng, *Israel Journal of Chemistry*, 2017, **57**, 586-601.
29. T. Takahashi and H. Mihara, *Chemical Communications*, 2012, **48**, 1568-1570.
30. J. Bieschke, M. Herbst, T. Wiglenda, R. P. Friedrich, A. Boeddrich, F. Schiele, D. Kleckers, J. M. L. del Amo, B. A. Grüning and Q. Wang, *Nature chemical biology*, 2012, **8**, 93-101.
31. D. J. Hayne, S. Lim and P. S. Donnelly, *Chemical Society Reviews*, 2014, **43**, 6701-6715.
32. C. Wu, M. Biancalana, S. Koide and J.-E. Shea, *Journal of molecular biology*, 2009, **394**, 627-633.
33. P. P. N. Rao, T. Mohamed, K. Teckwani and G. Tin, *Chemical Biology & Drug Design*, 2015, **86**, 813-820.
34. C. Rodríguez-Rodríguez, A. Rimola, L. Rodríguez-Santiago, P. Ugliengo, A. Alvarez-Larena, H. Gutiérrez-de-Terán, M. Sodupe and P. González-Duarte, *Chemical Communications*, 2010, **46**, 1156-1158.
35. D. Ding, K. Li, B. Liu and B. Z. Tang, *Accounts of Chemical Research*, 2013, **46**, 2441-2453.
36. Y. Yang, S. Li, Q. Zhang, Y. Kuang, A. Qin, M. Gao, F. Li and B. Z. Tang, *Journal of Materials Chemistry B*, 2019, **7**, 2434-2441.
37. K. P. R. Nilsson, P. Hammarström, F. Ahlgren, A. Herland, E. A. Schnell, M. Lindgren, G. T. Westermark and O. Inganäs, *ChemBioChem*, 2006, **7**, 1096-1104.
38. K. Rajasekhar, N. Narayanaswamy, N. A. Murugan, G. Kuang, H. Ågren and T. Govindaraju, *Scientific reports*, 2016, **6**, 23668.
39. P. S. Vassar and C. Culling, *Archives of pathology*, 1959, **68**, 487-498.
40. W. E. Klunk, Y. Wang, G.-f. Huang, M. L. Debnath, D. P. Holt and C. A. Mathis, *Life Sciences*, 2001, **69**, 1471-1484.
41. E. E. Nesterov, J. Skoch, B. T. Hyman, W. E. Klunk, B. J. Bacskai and T. M. Swager, *Angewandte Chemie International Edition*, 2005, **44**, 5452-5456.
42. M. Ono, M. Ishikawa, H. Kimura, S. Hayashi, K. Matsumura, H. Watanabe, Y. Shimizu, Y. Cheng, M. Cui, H. Kawashima and H. Saji, *Bioorganic & Medicinal Chemistry Letters*, 2010, **20**, 3885-3888.
43. M. Cui, M. Ono, H. Watanabe, H. Kimura, B. Liu and H. Saji, *Journal of the American Chemical Society*, 2014, **136**, 3388-3394.
44. M. Ono, H. Watanabe, H. Kimura and H. Saji, *ACS Chemical Neuroscience*, 2012, **3**, 319-324.
45. C. Ran, X. Xu, S. B. Raymond, B. J. Ferrara, K. Neal, B. J. Bacskai, Z. Medarova and A. Moore, *Journal of the American Chemical Society*, 2009, **131**, 15257-15261.
46. N. H. Mudliar and P. K. Singh, *Chemical communications*, 2019, **55**, 3907-3910.
47. C. W. T. Leung, F. Guo, Y. Hong, E. Zhao, R. T. K. Kwok, N. L. C. Leung, S. Chen, N. N. Vaikath, O. M. El-Agnaf and Y. Tang, *Chemical Communications*, 2015, **51**, 1866-1869.
48. W. Fu, C. Yan, Z. Guo, J. Zhang, H. Zhang, H. Tian and W.-H. Zhu, *Journal of the American Chemical Society*, 2019, **141**, 3171-3177.
49. C. L. Teoh, D. Su, S. Sahu, S.-W. Yun, E. Drummond, F. Prelli, S. Lim, S. Cho, S. Ham, T. Wisniewski and Y.-T. Chang, *Journal of the American Chemical Society*, 2015, **137**, 13503-13509.
50. J.-X. Wang, Y. Zhuo, Y. Zhou, H.-J. Wang, R. Yuan and Y.-Q. Chai, *ACS Applied Materials & Interfaces*, 2016, **8**, 12968-12975.

51. Y. Jia, L. Yang, R. Feng, H. Ma, D. Fan, T. Yan, R. Feng, B. Du and Q. Wei, *ACS applied materials & interfaces*, 2019, **11**, 7157-7163.
52. G. Zhao, Y. Wang, X. Li, Q. Yue, X. Dong, B. Du, W. Cao and Q. Wei, *Analytical Chemistry*, 2019, **91**, 1989-1996.
53. Y. Zhang, G. Figueroa-Miranda, Z. Lyu, C. Zafiu, D. Willbold, A. Offenhäusser and D. Mayer, *Sensors and Actuators B: Chemical*, 2019, **288**, 535-542.
54. H. Qin, X. Gao, X. Yang, W. Cao and S. Liu, *Biosensors and Bioelectronics*, 2019, **141**, 111438.
55. J. Qin, M. Cho and Y. Lee, *Analytical Chemistry*, 2019, **91**, 11259-11265.
56. J. Qin, J. S. Park, D. G. Jo, M. Cho and Y. Lee, *Sensors and Actuators B: Chemical*, 2018, **273**, 1593-1599.
57. S. Wustoni, S. Wang, J. R. Alvarez, T. C. Hidalgo, S. P. Nunes and S. Inal, *Biosensors and Bioelectronics*, 2019, **143**, 111561.
58. N. Xia, X. Wang, B. Zhou, Y. Wu, W. Mao and L. Liu, *ACS Applied Materials & Interfaces*, 2016, **8**, 19303-19311.
59. H. T. Beier, C. B. Cowan, I. H. Chou, J. Pallikal, J. E. Henry, M. E. Benford, J. B. Jackson, T. A. Good and G. L. Coté, *Plasmonics*, 2007, **2**, 55-64.
60. J.-K. Yang, I.-J. Hwang, M. G. Cha, H.-I. Kim, D. Yim, D. H. Jeong, Y.-S. Lee and J.-H. Kim, *Small*, 2019, **15**, 1900613.
61. X. Zhang, S. Liu, X. Song, H. Wang, J. Wang, Y. Wang, J. Huang and J. Yu, *ACS Sensors*, 2019, **4**, 2140-2149.
62. Y. Xia, P. Padmanabhan, S. Sarangapani, B. Gulyás and M. Vadakke Matham, *Scientific Reports*, 2019, **9**, 8497.
63. Y. Zhou, H. Dong, L. Liu and M. Xu, *Small*, 2015, **11**, 2144-2149.
64. N. Xia, B. Zhou, N. Huang, M. Jiang, J. Zhang and L. Liu, *Biosensors and Bioelectronics*, 2016, **85**, 625-632.
65. K. Tsukakoshi, K. Abe, K. Sode and K. Ikebukuro, *Analytical chemistry*, 2012, **84**, 5542-5547.
66. F. Ylera, R. Lurz, V. A. Erdmann and J. P. Fürste, *Biochemical and Biophysical Research Communications*, 2002, **290**, 1583-1588.
67. B. Chakravarthy, M. Ménard, L. Brown, M. Hewitt, T. Atkinson and J. Whitfield, *Journal of neurochemistry*, 2013, **126**, 415-424.
68. E. Andreetto, L. M. Yan, M. Taterek - Nossol, A. Velkova, R. Frank and A. Kapurniotu, *Angewandte Chemie International Edition*, 2010, **49**, 3081-3085.
69. Q. Wang, G. Liang, M. Zhang, J. Zhao, K. Patel, X. Yu, C. Zhao, B. Ding, G. Zhang, F. Zhou and J. Zheng, *ACS Chemical Neuroscience*, 2014, **5**, 972-981.
70. C. Hock, U. Konietzko, A. Papassotiropoulos, A. Wollmer, J. Streffer, R. C. von Rotz, G. Davey, E. Moritz and R. M. Nitsch, *Nature medicine*, 2002, **8**, 1270-1275.
71. B. O'Nuallain and R. Wetzell, *Proceedings of the National Academy of Sciences*, 2002, **99**, 1485-1490.
72. W. E. Klunk, H. Engler, A. Nordberg, Y. Wang, G. Blomqvist, D. P. Holt, M. Bergström, I. Savitcheva, G. F. Huang and S. Estrada, *Annals of Neurology: Official Journal of the American Neurological Association and the Child Neurology Society*, 2004, **55**, 306-319.
73. C. Hock, U. Konietzko, J. R. Streffer, J. Tracy, A. Signorell, B. Müller-Tillmanns, U. Lemke, K. Henke, E. Moritz, E. Garcia, M. A. Wollmer, D. Umbricht, D. J. F. de Quervain, M. Hofmann, A. Maddalena, A. Papassotiropoulos and R. M. Nitsch, *Neuron*, 2003, **38**, 547-554.



74. A. Nabers, J. Ollesch, J. Schartner, C. Kötting, J. Genius, H. Hafermann, H. Klafki, K. Gerwert and J. Wiltfang, *Analytical Chemistry*, 2016, **88**, 2755-2762.
75. D. Schenk, M. Hagen and P. Seubert, *Current opinion in immunology*, 2004, **16**, 599-606.
76. M. M. Dorostkar, S. Burgold, S. Filser, S. Barghorn, B. Schmidt, U. R. Anumala, H. Hillen, C. Klein and J. Herms, *Brain*, 2014, **137**, 3319-3326.
77. D. Schenk, R. Barbour, W. Dunn, G. Gordon, H. Grajeda, T. Guido, K. Hu, J. Huang, K. Johnson-Wood and K. Khan, *Nature*, 1999, **400**, 173-177.
78. S. G. Younkin, *Nature medicine*, 2001, **7**, 18-19.
79. Y. Du, R. Dodel, H. Hampel, K. Buerger, S. Lin, B. Eastwood, K. Bales, F. Gao, H. J. Moeller and W. Oertel, *Neurology*, 2001, **57**, 801-805.
80. V. Geylis, V. Kourilov, Z. Meiner, I. Nennesmo, N. Bogdanovic and M. Steinitz, *Neurobiology of aging*, 2005, **26**, 597-606.
81. K. L. Youmans, L. M. Tai, T. Kanekiyo, W. B. Stine Jr, S.-C. Michon, E. Nwabuisi-Heath, A. M. Manelli, Y. Fu, S. Riordan and W. A. Eimer, *Molecular neurodegeneration*, 2012, **7**, 8.
82. R. Kaye, E. Head, F. Sarsoza, T. Saing, C. W. Cotman, M. Necula, L. Margol, J. Wu, L. Breydo and J. L. Thompson, *Molecular neurodegeneration*, 2007, **2**, 18.
83. A. Bonito - Oliva, S. Schedin - Weiss, S. S. Younesi, A. Tiiman, C. Adura, N. Paknejad, M. Brendel, Y. Romin, R. J. Parchem and C. Graff, *Journal of cellular and molecular medicine*, 2019, **23**, 2103-2114.
84. M. J. Guerrero-Muñoz, D. L. Castillo-Carranza, S. Krishnamurthy, A. A. Paulucci-Holthausen, U. Sengupta, C. A. Lasagna-Reeves, Y. Ahmad, G. R. Jackson and R. Kaye, *Neurobiology of disease*, 2014, **71**, 14-23.
85. D. M. Hartley, D. M. Walsh, P. Y. Chianping, T. Diehl, S. Vasquez, P. M. Vassilev, D. B. Teplow and D. J. Selkoe, *Journal of Neuroscience*, 1999, **19**, 8876-8884.
86. A. D. Ellington and J. W. Szostak, *Nature*, 1990, **346**, 818-822.
87. D. H. Bunka and P. G. Stockley, *Nature Reviews Microbiology*, 2006, **4**, 588-596.
88. X. Ren, Y. Zhao, F. Xue, Y. Zheng, H. Huang, W. Wang, Y. Chang, H. Yang and J. Zhang, *Molecular Therapy-Nucleic Acids*, 2019, **17**, 726-740.
89. T. Mashima, F. Nishikawa, Y. O. Kamatari, H. Fujiwara, M. Saimura, T. Nagata, T. Kodaki, S. Nishikawa, K. Kuwata and M. Katahira, *Nucleic acids research*, 2012, **41**, 1355-1362.
90. A. Miodek, A. Poturnayová, M. Šnejdárková, T. Hianik and H. Korri-Youssoufi, *Analytical and bioanalytical chemistry*, 2013, **405**, 2505-2514.
91. S. Lisi, E. Fiore, S. Scarano, E. Pascale, Y. Boehman, F. Duconge, S. Chierici, M. Minunni, E. Peyrin and C. Ravelet, *Analytica chimica acta*, 2018, **1038**, 173-181.
92. J. H. Kim, E. Kim, W. H. Choi, J. Lee, J. H. Lee, H. Lee, D.-E. Kim, Y. H. Suh and M. J. Lee, *Molecular pharmaceuticals*, 2016, **13**, 2039-2048.
93. O. V. Galzitskaya, *Molecular BioSystems*, 2015, **11**, 2210-2218.
94. D. H. Bunka, B. J. Mantle, I. J. Morten, G. A. Tennent, S. E. Radford and P. G. Stockley, *Journal of Biological Chemistry*, 2007, **282**, 34500-34509.
95. F. Rahimi, K. Murakami, J. L. Summers, C.-H. B. Chen and G. Bitan, *PloS one*, 2009, **4**, e7694.
96. E. M. McConnell, M. R. Holahan and M. C. DeRosa, *Nucleic acid therapeutics*, 2014, **24**, 388-404.
97. T. Takahashi, K. Tada and H. Mihara, *Molecular BioSystems*, 2009, **5**, 986-991.
98. Y. Mazor, S. Gilead, I. Benhar and E. Gazit, *Journal of molecular biology*, 2002, **322**, 1013-1024.

99. B. Chakravarthy, S. Ito, T. Atkinson, C. Gaudet, M. Ménard, L. Brown and J. Whitfield, *Biochemical and biophysical research communications*, 2014, **445**, 656-660.
100. L. O. Tjernberg, J. Näslund, F. Lindqvist, J. Johansson, A. R. Karlström, J. Thyberg, L. Terenius and C. Nordstedt, *Journal of Biological Chemistry*, 1996, **271**, 8545-8548.
101. M. M. Gessel, C. Wu, H. Li, G. Bitan, J.-E. Shea and M. T. Bowers, *Biochemistry*, 2011, **51**, 108-117.
102. N. Xiong, X.-Y. Dong, J. Zheng, F.-F. Liu and Y. Sun, *ACS applied materials & interfaces*, 2015, **7**, 5650-5662.
103. G. Zhao, F. Qi, X. Dong, J. Zheng and Y. Sun, *Reactive and Functional Polymers*, 2019, **140**, 72-81.
104. F. Yang, G. P. Lim, A. N. Begum, O. J. Ubeda, M. R. Simmons, S. S. Ambegaokar, P. P. Chen, R. Kaye, C. G. Glabe and S. A. Frautschy, *Journal of Biological Chemistry*, 2005, **280**, 5892-5901.
105. Y. Feng, X.-p. Wang, S.-g. Yang, Y.-j. Wang, X. Zhang, X.-t. Du, X.-x. Sun, M. Zhao, L. Huang and R.-t. Liu, *Neurotoxicology*, 2009, **30**, 986-995.
106. H. Xie, J.-R. Wang, L.-F. Yau, Y. Liu, L. Liu, Q.-B. Han, Z. Zhao and Z.-H. Jiang, *Molecules*, 2014, **19**, 5119-5134.
107. B. Ren, Y. Liu, Y. Zhang, Y. Cai, X. Gong, Y. Chang, L. Xu and J. Zheng, *ACS Chemical Neuroscience*, 2018, **9**, 1215-1224.
108. B. Ren, Y. Liu, Y. Zhang, M. Zhang, Y. Sun, G. Liang, J. Xu and J. Zheng, *Journal of Materials Chemistry B*, 2018, **6**, 56-67.
109. A. Lorenzo and B. A. Yankner, *Proceedings of the National Academy of Sciences*, 1994, **91**, 12243-12247.
110. D. Morshedi, N. Rezaei - Ghaleh, A. Ebrahim - Habibi, S. Ahmadian and M. Nemat - Gorgani, *The FEBS journal*, 2007, **274**, 6415-6425.
111. M. Ionov, V. Burchell, B. Klajnert, M. Bryszewska and A. Abramov, *Neuroscience*, 2011, **180**, 229-237.
112. G. KELIÉNYI, *Journal of Histochemistry & Cytochemistry*, 1967, **15**, 172-180.
113. H. Puchtler, F. Sweat and M. Levine, *Journal of Histochemistry & Cytochemistry*, 1962, **10**, 355-364.
114. N. Pradhan, D. Jana, B. K. Ghorai and N. R. Jana, *ACS Applied Materials & Interfaces*, 2015, **7**, 25813-25820.
115. Y.-L. Wang, C. Fan, B. Xin, J.-P. Zhang, T. Luo, Z.-Q. Chen, Q.-Y. Zhou, Q. Yu, X.-N. Li, Z.-L. Huang, C. Li, M.-Q. Zhu and B. Z. Tang, *Materials Chemistry Frontiers*, 2018, **2**, 1554-1562.
116. A. K. Buell, E. K. Esbjörner, P. J. Riss, D. A. White, F. I. Aigbirhio, G. Toth, M. E. Welland, C. M. Dobson and T. P. Knowles, *Physical Chemistry Chemical Physics*, 2011, **13**, 20044-20052.
117. A. K. Buell, C. M. Dobson, T. P. J. Knowles and M. E. Welland, *Biophysical Journal*, 2010, **99**, 3492-3497.
118. Q. Wang, X. Yu, K. Patal, R. Hu, S. Chuang, G. Zhang and J. Zheng, *ACS Chemical Neuroscience*, 2013, **4**, 1004-1015.
119. M. R. Brier, B. Gordon, K. Friedrichsen, J. McCarthy, A. Stern, J. Christensen, C. Owen, P. Aldea, Y. Su, J. Hassenstab, N. J. Cairns, D. M. Holtzman, A. M. Fagan, J. C. Morris, T. L. S. Benzinger and B. M. Ances, *Science Translational Medicine*, 2016, **8**, 338ra366.
120. T. Hu, C. Chen, G. Huang and X. Yang, *Sensors and Actuators B: Chemical*, 2016, **234**, 63-69.
121. L. Sasso, S. Suei, L. Domigan, J. Healy, V. Nock, M. Williams and J. Gerrard, *Nanoscale*, 2014, **6**,

- 1629-1634.
122. X. Zhu, N. Zhang, Y. Zhang, B. Liu, Z. Chang, Y. Zhou, Y. Hao, B. Ye and M. Xu, *Analytical methods*, 2018, **10**, 641-645.
123. C. Lou, T. Jing, J. Zhou, J. Tian, Y. Zheng, C. Wang, Z. Zhao, J. Lin, H. Liu and C. Zhao, *International Journal of Biological Macromolecules*, 2020, **149**, 1130-1138.
124. C. Lou, T. Jing, J. Tian, Y. Zheng, J. Zhang, M. Dong, C. Wang, C. Hou, J. Fan and Z. Guo, *Journal of Materials Research*, 2019, **34**, 2964-2975.
125. C. A. Mathis, B. J. Bacskai, S. T. Kajdasz, M. E. McLellan, M. P. Frosch, B. T. Hyman, D. P. Holt, Y. Wang, G.-F. Huang and M. L. Debnath, *Bioorganic & medicinal chemistry letters*, 2002, **12**, 295-298.
126. C. Xia and B. C. Dickerson, *PET clinics*, 2017, **12**, 351-359.
127. G. Sundaram, D. D. Dhavale, J. L. Prior, P. Yan, J. Cirrito, N. P. Rath, R. Laforest, N. J. Cairns, J.-M. Lee and P. T. Kotzbauer, *Scientific reports*, 2016, **6**, 35636.
128. V. L. Villemagne, K. Ong, R. S. Mulligan, G. Holl, S. Pejoska, G. Jones, G. O'Keefe, U. Ackerman, H. Tochon-Danguy and J. G. Chan, *Journal of Nuclear Medicine*, 2011, **52**, 1210-1217.
129. S. M. Landau, A. Fero, S. L. Baker, R. Koeppe, M. Mintun, K. Chen, E. M. Reiman and W. J. Jagust, *Journal of Nuclear Medicine*, 2015, **56**, 567-574.
130. V. Camus, P. Payoux, L. Barré, B. Desgranges, T. Voisin, C. Tauber, R. La Joie, M. Tafani, C. Hommet and G. Chételat, *European journal of nuclear medicine and molecular imaging*, 2012, **39**, 621-631.
131. H. Naiki, K. Higuchi, M. Hosokawa and T. Takeda, *Analytical Biochemistry*, 1989, **177**, 244-249.
132. C. Gan, L. Zhou, Z. Zhao and H. Wang, *Medicinal chemistry research*, 2013, **22**, 4069-4074.
133. L. P. Jameson and S. V. Dzyuba, *Bioorganic & medicinal chemistry letters*, 2013, **23**, 1732-1735.
134. X. Zhang, Y. Tian, C. Zhang, X. Tian, A. W. Ross, R. D. Moir, H. Sun, R. E. Tanzi, A. Moore and C. Ran, *Proceedings of the National Academy of Sciences*, 2015, **112**, 9734-9739.
135. K. Zhou, C. Yuan, B. Dai, K. Wang, Y. Chen, D. Ma, J. Dai, Y. Liang, H. Tan and M. Cui, *Journal of Medicinal Chemistry*, 2019, **62**, 6694-6704.
136. J.-D. Zhang, J. Mei, X.-L. Hu, X.-P. He and H. Tian, *Small*, 2016, **12**, 6562-6567.
137. D. J. Selkoe and J. Hardy, *EMBO molecular medicine*, 2016, **8**, 595-608.
138. N. D. Younan and J. H. Viles, *Biochemistry*, 2015, **54**, 4297-4306.
139. K. Liu, T. L. Guo, J. Chojnacki, H.-G. Lee, X. Wang, S. L. Siedlak, W. Rao, X. Zhu and S. Zhang, *ACS chemical neuroscience*, 2012, **3**, 141-146.
140. A. M. Fanni, F. A. Monge, C.-Y. Lin, A. Thapa, K. Bhaskar, D. G. Whitten and E. Y. Chi, *ACS Chemical Neuroscience*, 2019, **10**, 1813-1825.
141. J. Han, M. Zhang, G. Chen, Y. Zhang, Q. Wei, Y. Zhuo, G. Xie, R. Yuan and S. Chen, *Journal of Materials Chemistry B*, 2017, **5**, 8330-8336.
142. C. Wang, N. Zhang, Y. Li, L. Yang, D. Wei, T. Yan, H. Ju, B. Du and Q. Wei, *Sensors and Actuators B: Chemical*, 2019, **291**, 319-328.
143. J. Fang, G. Zhao, X. Dong, X. Li, J. Miao, Q. Wei and W. Cao, *Biosensors and Bioelectronics*, 2019, **142**, 111517.
144. Y. Wang, Y. Zhang, H. Sha, X. Xiong and N. Jia, *ACS Applied Materials & Interfaces*, 2019, **11**, 36299-36306.
145. M. Masářík, A. Stobiecka, R. Kizek, F. Jelen, Z. Pechan, W. Hoyer, T. M. Jovin, V. Subramaniam and E. Paleček, *Electroanalysis: An International Journal Devoted to Fundamental and Practical*

- Aspects of Electroanalysis*, 2004, **16**, 1172-1181.
146. M. d. Vestergaard, K. Kerman, M. Saito, N. Nagatani, Y. Takamura and E. Tamiya, *Journal of the American Chemical Society*, 2005, **127**, 11892-11893.
147. M. Faure, F. Billon, I. Le Potier, A.-M. Haghiri-Gosnet, B. Tribollet, A. Pailleret, C. Deslouis and J. Gamby, *Electrochimica Acta*, 2019, **296**, 251-258.
148. M. Chikae, T. Fukuda, K. Kerman, K. Idegami, Y. Miura and E. Tamiya, *Bioelectrochemistry*, 2008, **74**, 118-123.
149. Y. Zhou, H. Zhang, L. Liu, C. Li, Z. Chang, X. Zhu, B. Ye and M. Xu, *Scientific reports*, 2016, **6**, 35186.
150. L. Liu, N. Xia, M. Jiang, N. Huang, S. Guo, S. Li and S. Zhang, *Journal of Electroanalytical Chemistry*, 2015, **754**, 40-45.
151. E. C. Rama, M. B. González-García and A. Costa-García, *Sensors and Actuators B: Chemical*, 2014, **201**, 567-571.
152. E. Protopapa, S. Maude, A. Aggeli and A. Nelson, *Langmuir*, 2009, **25**, 3289-3296.
153. L. Liu, Q. He, F. Zhao, N. Xia, H. Liu, S. Li, R. Liu and H. Zhang, *Biosensors and Bioelectronics*, 2014, **51**, 208-212.
154. S. Hrapovic, Y. Liu, K. B. Male and J. H. Luong, *Analytical chemistry*, 2004, **76**, 1083-1088.
155. B. Zhang, B. Liu, J. Zhou, J. Tang and D. Tang, *ACS Applied Materials & Interfaces*, 2013, **5**, 4479-4485.
156. M. Wang, Z. Fu, B. Li, Y. Zhou, H. Yin and S. Ai, *Analytical chemistry*, 2014, **86**, 5606-5610.
157. A. J. Veloso, V. W. S. Hung, G. Sindhu, A. Constantinof and K. Kerman, *Analytical chemistry*, 2009, **81**, 9410-9415.
158. A. J. Veloso, T. Chan, V. Wing Sze Hung, L. Lam and K. Kerman, *Electroanalysis*, 2011, **23**, 2753-2756.
159. W. A. El - Said, K. Abd El - Hameed, N. Abo El - Maali and H. G. Sayyed, *Electroanalysis*, 2017, **29**, 748-755.
160. H. Li, Y. Cao, X. Wu, Z. Ye and G. Li, *Talanta*, 2012, **93**, 358-363.
161. H. Li, H. Xie, Y. Cao, X. Ding, Y. Yin and G. Li, *Analytical Chemistry*, 2013, **85**, 1047-1052.
162. L. Liu, F. Zhao, F. Ma, L. Zhang, S. Yang and N. Xia, *Biosensors and Bioelectronics*, 2013, **49**, 231-235.
163. S. Prabhulkar, R. Piatyszek, J. R. Cirrito, Z. Z. Wu and C. Z. Li, *Journal of neurochemistry*, 2012, **122**, 374-381.
164. H. Liu, X. Zhou, Q. Shen and D. Xing, *Theranostics*, 2018, **8**, 2289.
165. M. Moskovits, *Reviews of modern physics*, 1985, **57**, 783-826.
166. E. J. Blackie, E. C. Le Ru and P. G. Etchegoin, *Journal of the American Chemical Society*, 2009, **131**, 14466-14472.
167. L. Gao, L. Zhang, X. Lyu, G. Lu and Q. Liu, *Eng. Sci*, 2018, **1**, 69-77.
168. D. Liu, Z. Wang and X. Jiang, *Nanoscale*, 2011, **3**, 1421-1433.
169. X. Xu, J. Zhang, F. Yang and X. Yang, *Chemical Communications*, 2011, **47**, 9435-9437.
170. R. Elghanian, J. J. Storhoff, R. C. Mucic, R. L. Letsinger and C. A. Mirkin, *Science*, 1997, **277**, 1078.
171. H. Wei, B. Li, J. Li, E. Wang and S. Dong, *Chemical Communications*, 2007, 3735-3737.
172. T. Hu, S. Lu, C. Chen, J. Sun and X. Yang, *Sensors and Actuators B: Chemical*, 2017, **243**, 792-799.

173. Y. Yu, L. Zhang, X. Sun, C. Li, Y. Qiu, H. Sun, D. Tang, Y. Liu and X. Yin, *Chemical Communications*, 2015, **51**, 8880-8883.
174. N. Mattsson, H. Zetterberg, S. Janelidze, P. S. Insel, U. Andreasson, E. Stomrud, S. Palmqvist, D. Baker, C. A. T. Hehir and A. Jeromin, *Neurology*, 2016, **87**, 1827-1835.